Numerical Weather Prediction

Volcanic SO_2 detection by satellite using infrared radiometers

Forecasting Research Technical Report No. 487

Marie Doutriaux-Boucher, P. Dubuisson, R. Saunders, and S. Watkin

email: nwp_publications@metoffice.gov.uk

©Crown Copyright

Volcanic SO_2 detection by satellite using IR instruments

Marie Doutriaux-Boucher, Roger Saunders, and Sarah Watkin
MetOffice, FitzRoy Road, Exeter, EX1 3PB, U.K.

Philippe Dubuisson
Université du Littoral, Station Marine de Wimereux, 62930 Wimereux, France.

Document History

Date	Version	Action	Approval
11/4/2006	1.0	First version of the report	R. Saunders
31/5/2006	2.0	Amended version of the report	R. Saunders
20/6/2006	3.0	Amended version of the report	J. Eyre
08/9/2006	4.0	Final version	R. Saunders

Table of contents

1. Introduction 4
2. SO_2 detection from space 5
2.1 Generalities 5
2.2 MSG instrument and SO_2 6
2.3 MODIS instrument and SO_2 7
3. Different existing retrieval techniques 8
3.1 Realmuto, one channel technique 8
3.2 Schreiner, two channel technique 8
3.3 Prata, three channel technique 8
4. Theoretical investigation in the retrieval technique. 9
4.1 Planck function and radiance units 9
4.2 Radiative transfer simulations 11
4.2.1 Impact of the water vapour content on the retrieval algorithm 13
4.2.2 Impact of cirrus clouds on the retrieval algorithm 15
5. Case studies from MODIS measurements 17
5.1 Brief description of the different volcanoes 17
5.2 Results 18
6. Possible exploitation of SEVIRI 21
6.1 Comparison of MODIS and SEVIRI channels 21
6.2 Example of SEVIRI retrieval 23
7. Conclusions 25
References 27
Appendix 1: SO_2 detection figures 30
Appendix 2: SO_2 quantity units. 34
A.1 Definition 34
A.2 Conversion from ppmv to DU 34
Appendix 3: Interesting websites 35

1. Introduction

This report is a follow-up of a work on volcanic ash detection (Watkin 2005). As ash is not always detected from space, SO_2 can be used as another marker for a volcanic eruption and presence of ash in the vicinity. In that respect, SO_2 detection from space can be very useful for civil aviation, helping air traffic to avoid volcanic eruptions.

Usually more than 50 volcanoes erupt each year (Andres and Kasgnoc, 1998). They have different behaviours from continuous activity to a low frequency of eruption. During an eruption, a volcano produces large amount of aerosols and several gas species. This creates hazardous conditions for passing aircraft and the potential for significant climate effects. The most prevalent gases are water vapour, carbon dioxide, sulphur dioxide (SO_2), and hydrogen sulphide (H_2S). The estimate of the global volcanic SO_2 flux is around 7.5-10.5 Tg/yr (Pugnaghi et al. 2006). This corresponds to 10-15% of the annual anthropogenic sulphur emissions (Halmer et al. 2002). This report will focus on SO_2 detection. Sulphur dioxide can cause significant damage to the local environment and, if in high concentrations, to human health. It can also perturb the climate and the atmosphere through the action of sulphate aerosols (Lacis et al., 1992). For these various reasons, it is important to monitor volcanic emissions. Direct measurements of emitted volcanic gases is a dangerous task, therefore remote sensing is a useful complementary tool. A good summary of volcanic cloud detection from satellite remote sensing is made in Rose et al. (2000).

Sulphur dioxide is found at different levels of the atmosphere, from the troposphere to the stratosphere. The lifetime of volcanic SO_2 in the atmosphere depends on the height of the eruption. In the troposphere it ranges from less than a day to a few days. It is removed from the atmosphere by different processes. In the gaseous phase, SO_2 will be removed by oxidation by OH to form H_2SO_4, which then condenses to form aerosols. It can also be oxidised in aqueous phase in clouds. The concentration of SO_2 in the clear atmosphere is less than 1 ppbv, which corresponds to a total column density of 0.2 Dobson Unit (DU) in a boundary layer of 2 km (see appendix 2). SO_2 from volcanoes is one of the most important source of stratospheric aerosols. In the stratosphere, the lifetime of sulphur dioxide is several weeks during which it produces sulphuric acid vapour which condenses to form sulphuric acid aerosols (Baran et al. 1993). Sedimentation being the only sink in the stratosphere, the residence time of stratospheric aerosol can be as long as several years. This significantly increases the planetary albedo on climate time-scales.

Rose et al. (2000) explain that a volcanic cloud may have significantly higher SO_2 content on the second day of eruption as compared to the first day, suggesting that early volcanic emitted H_2S may be converting to SO_2. They also stated that in many cases, volcanic clouds separate into higher SO_2-rich portions and lower ash-rich portions. The two portions can follow different trajectories. So tracking ash will not necessarily indicate the presence of SO_2 and vice versa.

Detection of SO_2 is most commonly done on the surface using a portable correlation spectrometer COSPEC described by Rodriguez et al (2000). COSPEC takes advantage of the selective absorption of ultraviolet radiation between 300 and 330 nm. It converts the ultraviolet skylight transmitted through a plume into estimates of its SO_2 column. Other instruments operating at short wavelengths are Light Detection and Ranging (LIDAR) or differential absorption lidar (DIAL) and differential absorption spectroscopy (DOAS).

DIAL and DOAS enable the estimation of different concentration of trace gases (Weibring et al., 1998). Another ground based instrument used to monitor several atmospheric species is the Fourier Transform Infrared (FTIR) spectrometer (Francis et al., 1998).

2. SO_2 detection from space

2.1 Generalities

An absorption spectrum of SO_2 is shown in Figure 1. There are two absorption regions in the thermal infrared (IR), a strong absorption region due to the ν_3-band, between 1330-1390 cm^{-1} (wavelength around 7.3 µm) and a second, weaker, absorption region due to the ν_1-band, between 1160-1290 cm^{-1} (wavelength around 8.7 µm).

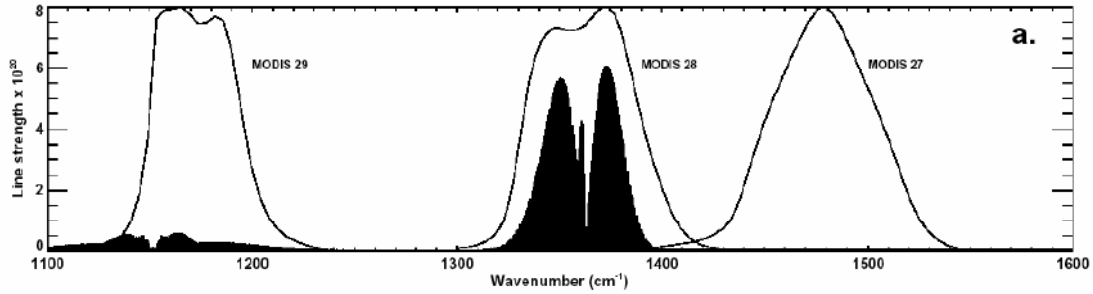

Figure 1: *MODIS channels and SO_2 absorption lines.*

As the detection from ground can be dangerous, remote sensing from space is very attractive. There are many space instruments that cover the 7.3 - 8.7 µm region of the atmospheric spectrum and can therefore detect SO_2 from space (e.g. HIRS/2-3, AIRS, MODIS, ASTER, SEVIRI). Figure 2 shows a non exhaustive list of such satellite instruments with their respective channels in the infrared spectrum.

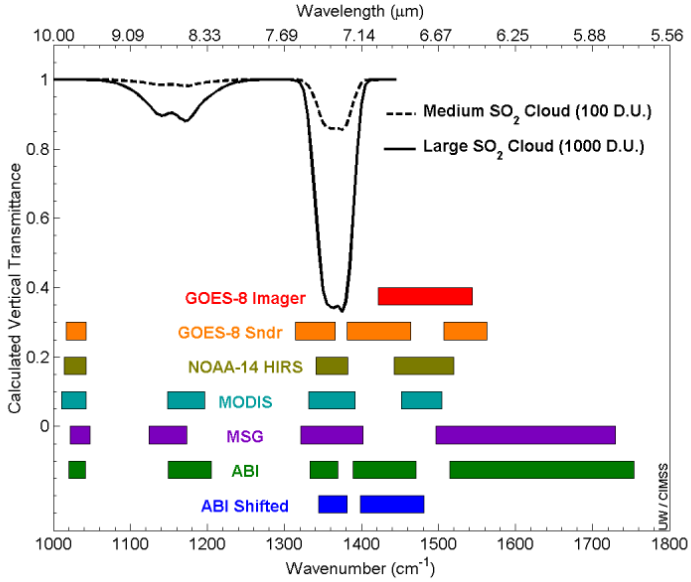

Figure 2: *Various satellite instruments channels and SO_2 transmittance.*

A SO_2 database from the Total Ozone Mapping Spectrometer (TOMS) measurements can be found at http://toms.umbc.edu/archives.html. It contains a list of eruptions seen by TOMS since 1978. The database currently contains 274 eruptive events from 70 volcanoes (see Figure 3). TOMS instrument measures backscattered ultraviolet radiance from Earth. It

was mainly designed and used to monitor the total column amount of ozone (O_3) globally. However, because SO_2 absorbs similarly to O_3 in the wavelengths used by TOMS, Krueger et al. (1983) developed a method to discriminate and quantify SO_2 columns. TOMS has been monitoring SO_2 for almost 30 years now (Krueger at al., 1995).

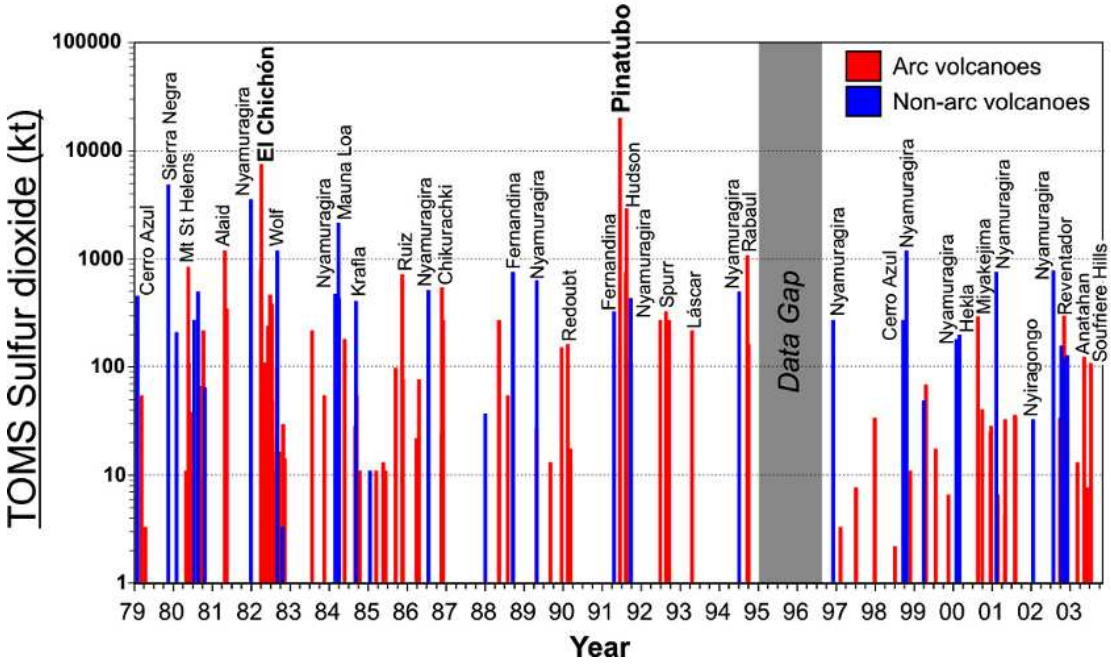

Figure 3: *Recent chart of TOMS volcanic SO2 against time, from the TOMS SO2 website, http://toms.umbc.edu/.*

2.2 MSG instrument and SO_2

Meteosat Second Generation (MSG) is a significantly enhanced follow-up system to the previous generation of Meteosat geostationary satellites. The first MSG satellite to be launched was Meteosat-8, in 2002. The second satellite followed in December 2005. The Spinning Enhanced Visible and InfraRed Imager of MSG (SEVIRI) has 12 spectral bands (as compared to only three in the previous system).

Channel	*Description*
1 – VIS06	Visible band centred on 0.6 µm
2 – VIS 0.8	Visible band centred on 0.8 µm
3 – IR1.6	Near-infrared window band centred on 1. 6 µm
4 – IR3.9	Infrared window band centred on 3.9 µm
5 – WV6.2	Water Vapour band centred on 6.2 µm
6 – WV7.3	Water Vapour band centred on 7.3 µm
7 – IR8.7	Infrared window band centred on 8.7 µm
8 – IR9.7	Ozone band centred on 9.7 µm
9 – IR10.8	Infrared window band centred on 10.8 µm
10 – IR12.0	Infrared window band centred on 12.0 µm
11 – IR13.4	CO_2 band centred on 13.4 µm
12 – HRV	Broadband high-resolution visible band

Table 1: *MSG channel description.*

Infrared spectral response functions of SEVIRI IR channels are shown in Figure 4. SEVIRI delivers images every 15 minutes, which is important for early detection of an eruption,

with a resolution of 3 km at sub-satellite point. The High Resolution Visible (HRV) channel has a resolution of 1 km.

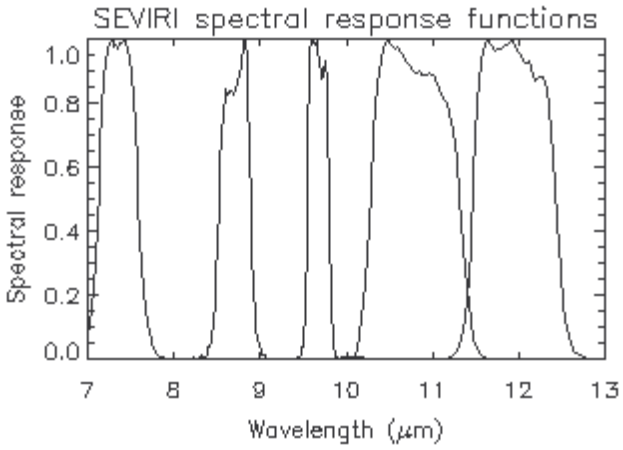

Figure 4 *SEVIRI spectral response functions in the SO_2 absorption regions of the spectrum.*

In theory MSG has the capability to detect SO_2 as channels 6 and 7 (respectively 7.3 and 8.6 μm) cover the SO_2 absorption bands shown in Figure 1. Unfortunately only one major eruption has occurred over the MSG disc during the first years of the MSG operational period (Soufriere, Montserrat Island 20 May 2006). Explosion of Mt. Karthala in Comoros on 24-26 November emitted little amount of SO_2. Therefore, to date, it has not been possible to test completely SO_2 retrieval schemes from MSG past data. Hence, in this study, we will focus on the MODIS satellite instrument to test available algorithms and we will present one case study using the MSG data.

2.3 MODIS instrument and SO_2

MODIS is another useful satellite instrument capable of retrieving SO_2 from space. MODIS has 36 spectral bands in the visible and infrared (from near to thermal) region of the spectrum (0.4-14.4 μm). Two of its bands operate at a nominal spatial resolution of 250 m at nadir, 5 bands at 500 m and the remaining bands at 1000 m. MODIS is now onboard two spacecraft: Terra, since December 1999, and Aqua, since May 2002. A ±55º field of view from nadir at 705 km altitude achieves a 2330 km swath and provides a near global coverage twice a day in the visible spectrum, and four times a day in the IR spectrum (http://modis.gsfc.nasa.gov).

MODIS band	8	3	4	1	6	7
Wavelength	405-420nm	459-479nm	545-565nm	620-670nm	1628-1652nm	2105-2155nm
MODIS band	20	21	22	25	27	28
Wavelength	3.660-3.840μm	3.929-3.989μm	3.939-3.989μm	4.482-4.549μm	6.535-6.895μm	7.175-7.475μm
MODIS band	29	30	31	32	36	
Wavelength	8.400-8.700μm	9.580-9.880μm	10.780-11.280μm	11.770-12.270μm	14.085-14.385μm	

Table 2: *MODIS wavebands available for volcanic SO_2 detection.*

Bands 28 and 29 of the MODIS instrument are located within SO_2 absorption bands (see Figure 1). They are the most suitable bands for SO_2 detection.

3. Different existing retrieval techniques

3.1 Realmuto, one channel technique

A first attempt to retrieve SO_2 from space was made using the airborne version of the MODIS instrument (airborne thermal infrared multispectral scanner TIMS) by Realmuto et al. (1994, 1997). The SO_2 retrieval was based on the used of radiative transfer codes (LOWTRAN and MODTRAN) which are used to model the radiance through an SO_2 plume as measured by TIMS at nadir. The presence of SO_2 in a plume results in the absorption and emission of radiance between 8 and 9.5 µm. The strength of the absorption and emission is a function of both SO_2 concentration and the temperature contrast between the plume and the ground. The radiative transfer modelling is used to find the concentration of SO_2 necessary to produce the observed attenuation of the radiance emitted at the ground. This technique could be applied to the 8.6 µm band of the MODIS instrument.

3.2 Schreiner, two channel technique

This technique has been used with the GOES sounder. It is described in Schneider et al. (2004). It uses the difference between the 7.3 µm water vapour and 13.3 µm CO_2 channels. The 13.3 µm band has been chosen because the weighting function (i.e. the region or vertical layer of the atmosphere where these spectral bands are most sensitive to change) for both bands peak around the same region of the atmosphere. Therefore the resulting derived image will in theory have subtracted the effects of the background temperature and more effectively portray the SO_2 plume. However the effects due to water vapour are not removed.

3.3 Prata, three channel technique

This technique is described in Prata et al. (2003) and Watson et al. (2004). It uses the fact that in the absence of SO_2 there is an approximate linear relationship between wavelength and radiances in the range of 6.8 to 10.8 µm. Radiances from these two channels can then be used to estimate the 7.3 µm radiance using equation (1):

$$R_{ch28est} = \left(R_{ch31} - R_{ch27}\right)\left(\frac{\lambda_{ch28} - \lambda_{ch27}}{\lambda_{ch31} - \lambda_{ch27}}\right) + R_{ch27} \quad (1)$$

Radiances are then converted to brightness temperatures using the Planck function. The difference between the estimated and the measured 7.3µm brightness temperature (BT) is sensitive to the SO_2 content. A positive difference between the 7.3 µm the estimated and observed BT indicates the presence of SO_2 in the atmospheric column. Figure 5 shows an idealised view of this method.

a) *b)*

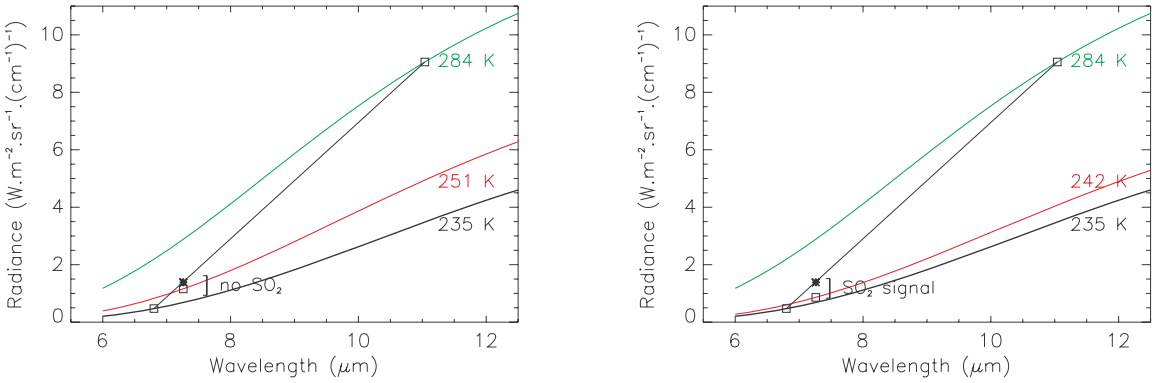

Figure 5: *Idealised view of the Prata SO_2 detection method. The squares represent the measured radiances at 6.8, 7.3 and 10.8 μm. The corresponding Planck functions are shown with solid lines. The interpolated radiance at 7.3 μm is represented by a star. The SO_2 presence is given by the difference between the linearly estimated radiance (converted to brightness temperature) at 7.3μm and the observed brightness temperature. Figures a) and b) correspond to an idealised case without and with SO_2, respectively.*

4. Theoretical investigation in the retrieval technique.

We decided to use a 3-channel retrieval technique similar to the one used by Prata but such a technique needs first to be laid on firmer theoretical grounds to understand its sensitivity and limitations. For this purpose, we have used simple considerations on the Planck function (section 4.1) and a sophisticated radiative transfer model to simulate various atmospheric conditions (section 4.2).

4.1 Planck function and radiance units

The Prata retrieval method uses the fact that the radiance is approximately linear between 6.8 and 10-11 µm. The radiance unit used in the retrieval appears to have a critical role. The Planck function provides the radiance emitted from a blackbody. The inverse of the Planck function is also used to derive the brightness temperature corresponding to a measured or simulated emitted radiance. The formula for the Planck function depends on whether the radiance is reckoned on a "per wavelength" basis, radiance unit being $Wm^{-2}sr^{-1}\mu m^{-1}$, or "per wavenumber" basis, radiance unit being $Wm^{-2}sr^{-1}(cm^{-1})^{-1}$. The two formulae are given in Table 3.

$B_\lambda(T) = \frac{2hc^2\lambda^{-5}}{\left(e^{\frac{hc}{k\lambda T}} - 1\right)}$ in $Wm^{-2}sr^{-1}\mu m^{-1}$	$B_\nu(T) = \frac{2h\nu^3c^2}{\left(e^{\frac{hc\nu}{kT}} - 1\right)}$ in $Wm^{-2}sr^{-1}(cm^{-1})^{-1}$
h, Planck constant , h= 6.626068.10^{-34} Js k, Boltzmann constant, k= 1.38066.10^{-23} JK^{-1} c, speed of light in vacuum, c= 2.997925.$10^{8}$$ms^{-1}$	

Table 3: *Planck function giving the radiance emitted by a "blackbody".*

Figure 6 illustrates the importance of the radiance unit used to retrieve the estimated radiance (or brightness temperature) at 7.3 µm. For temperatures above 260 K the maximum of the "per wavelength" radiance is located between 6.8 and 10.8 µm. So a linear interpolation using radiance in $Wm^{-2}sr^{-1}\mu m^{-1}$ should not be used for warm pixels and the radiance in $Wm^{-2}sr^{-1}(cm^{-1})^{-1}$ is preferable. For low temperatures the linearly interpolated radiance "per wavelength" will be a better estimate of the true radiance because the radiance "per wavenumber" is not quite linear between 6 and 10 µm, but this is not so critical.

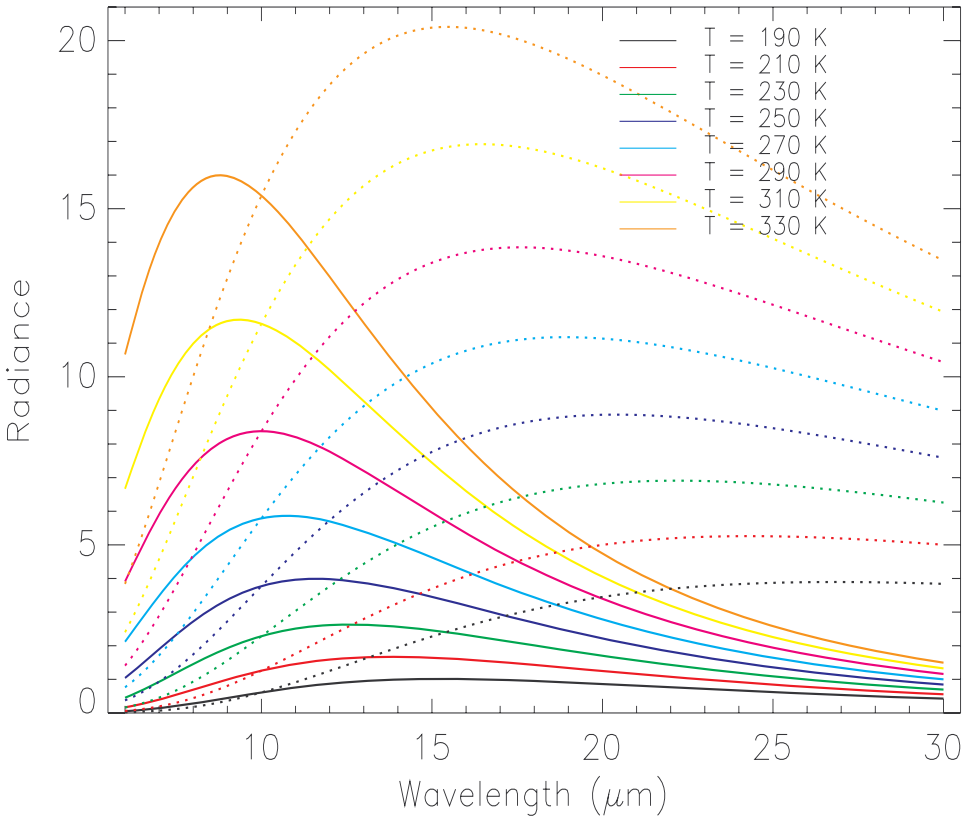

Figure 6: *Radiance retrieved for different brightness temperatures. The dotted lines represent radiance in $Wm^{-2}sr^{-1}(cm^{-1})^{-1}$ while plain lines represent radiance in $Wm^{-2}sr^{-1}\mu m^{-1}$.*

This is of course complicated by the fact that, for a real atmosphere, there is no single blackbody temperature. The 10.8 µm channel sees the surface and lower troposphere, 6.8 µm channel sees the upper troposphere and the 7.3 µm channel sees the lower troposphere. Therefore the 7.3 µm channel senses an atmospheric layer which lies in between the layers sensed by the 6.8 and 10.8 µm channels (Figure 5). This explains why the linear interpolation is still working.

In light of Figure 6 and the location of the Planck function maxima, we argue that the interpolation in units of $Wm^{-2}sr^{-1}(cm^{-1})^{-1}$ should be used.

4.2 Radiative transfer simulations

To understand what is happening in the MODIS SO_2 retrieval, we used a sophisticated line-by-line coupled with discrete ordinate radiative transfer model (LBLDOM). As SO_2 absorption is not easily included in radiative transfer codes currently used at the Met Office we used the LBLDOM model developed by Philippe Dubuisson from the University of Littoral in France. The radiances measured by MODIS or MSG in various channels can be accurately simulated using LBLDOM with high spectral resolution (Dubuisson et al., 1996; Dubuisson et al., 2005). This code solves the radiative transfer equation combining the Discrete Ordinate Method (DOM) (Stamnes et al., 1988) and a line-by-line model (LBL). Fluxes and radiances can be calculated at any atmospheric level in the solar and thermal spectral range, with a spectral resolution of about 0.0001 cm^{-1} in the longwave domain. The atmosphere is assumed to be vertically inhomogeneous and stratified into plane-parallel layers (40 layers are used in this study). Gaseous absorption is computed with the LBL code (Dubuisson et al., 1996) using the last version of the HITRAN spectroscopic database (Rothman et al., 2005). The shape and intensity of each absorption line is calculated as a function of the pressure and temperature using HITRAN database together with Lorentz, Doppler or Voigt profiles. CO_2 and H_2O absorption continua are computed using the CKD parameterization (Clough et al., 1989). Emitting and scattering processes, as well as their interactions with absorption, are calculated with the DOM. Clouds are defined with their spectral optical properties: optical thickness, single scattering albedo and moments of the Legendre polynomial decomposition of the phase function. The radiances computed at the top of the atmosphere with LBLDOM are converted into brightness temperatures in order to simulate MODIS or MSG measurements using conversion tables. Those tables are established in computing the radiance that would be measured by MODIS or MSG spectral filters for blackbodies with temperatures ranging from 150 to 350 K with a step of 1 K. A standard spline interpolation of those tables allows computing the brightness temperature that would be observed for any atmospheric conditions simulated by LBLDOM with an accuracy of a few hundredths of Kelvin.

It appears that there is no existing dataset of the vertical profile of SO_2 in the atmosphere for the case of volcanic eruptions. To use our radiative transfer model, we had to create three synthetic SO_2 profiles. These profiles show a maximum amount of SO_2 at different levels of the atmosphere as shown on Figure 7. The amount of SO_2 present in each column is constrained to be around 150 DU, to compare to the default amount of SO_2 present in an atmospheric column of 0.1 DU.

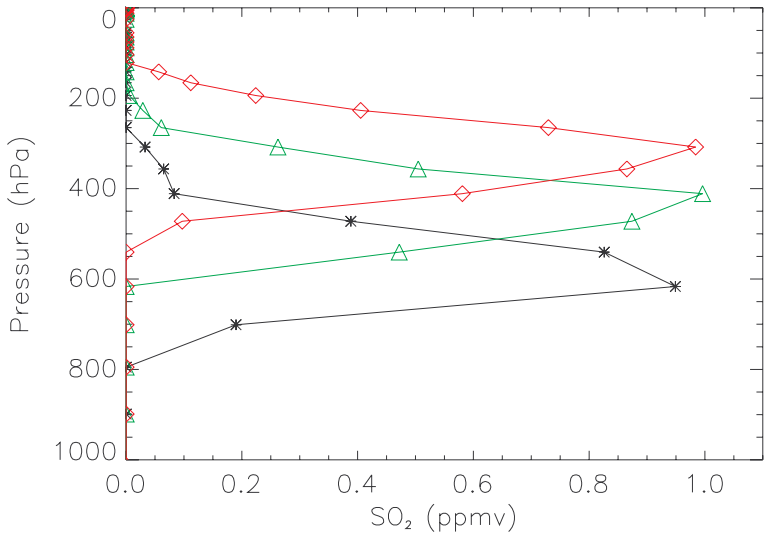

Figure 7: *Three empirical profiles of SO_2 in the atmosphere. Note that for each profile the total SO_2 amount present in the atmospheric column is 150 DU.*

This column SO_2 value has been chosen to be realistic. As shown from the TOMS/OMI SO_2 emission archive, for a very big eruption as the Pinatubo in 1991, the total SO_2 is around 300 DU (Guo et al., 2004), for a small one like Etna in 2002 around 20 DU was retrieved in a column (Carn et al., 2005). For an average eruption like the eruption of mount Hekla in 2000 (see Figure 3), the maximum SO_2 column abundance reported by TOMS was around 90 DU (Rose et al. 2003).

We use the LBLDOM model to compute the brightness temperature at the top of the atmosphere varying the SO_2 profiles. Two different atmospheric temperature profiles have been used. As a reference we used a standard profile and, as the London VAAC is looking after the Icelandic region, we used an Arctic atmospheric profile. Results of these simulations are shown in Table 4. As expected, looking at the differences in BTs obtained in simulations with SO_2 and simulation without SO_2, MODIS channels 28 and 29 and MSG channels 6 and 7 are the most sensitive to the SO_2 presence. From these simulations, we can infer that it will be easier to detect SO_2 when it is located higher in the atmosphere. Channel 30 of MODIS (mainly O_3 channel) is presented as well in Table 4 but is completely insensitive to SO_2. In theory it will be more difficult to detect SO_2 using MSG as the BT difference between no SO_2 and SO_2 simulations is smaller (6.5 K against 8 K for Arctic conditions at 7.3 μm).

	SO_2	MODIS 28	MODIS29	MODIS30	MSG 7.3	MSG 8.7
Reference atmospheric model profile 6 US Standard	no	252.98	284.65	270.36	253.56	284.89
	default	253.06	284.65	270.36	253.62	284.89
	600hPa	248.11	281.46	270.36	249.64	281.60
	400hPa	243.65	280.43	270.36	246.29	280.56
	300hPa	239.16	279.66	270.36	243.06	279.70
Arctic Profile	no	240.89	253.77	250.35	241.11	253.87
	default	240.93	253.77	250.35	241.14	253.87
	600hPa	238.15	252.65	250.35	238.94	252.72
	400hPa	234.43	251.60	250.35	236.09	251.66
	300hPa	232.24	250.87	250.35	234.45	250.92

Table 4: *Brightness temperature (K) simulated with LBLDOM model for two atmospheric profiles in MODIS and MSG channels sensitive to SO_2.*

4.2.1 Impact of the water vapour content on the retrieval algorithm

The effect of water vapour on the 3 channel retrieval was also investigated. We did some simulations for an atmosphere free of SO_2 but varying the water vapour content and the surface temperature. We interpolate the 7.3 µm radiance using the 6.8 and 10.8 µm and compare it to the computed 7.3 µm radiance. Under the assumption of the retrieval scheme these two values should be very similar (see Figure 5). Results are shown in Figure 8. Under all atmospheric conditions, the "observed" radiance at 7.3µm is reasonably similar to the linearly interpolated one (in per "wavenumber" unit). In clear sky conditions, differences of up to 3.5 K between the linearly estimated and the actual BT are retrieved. This implies that i) the linear relationship between radiances at 6.8 and 10.8 µm is not too sensitive to water vapour content and ii) we should not expect to retrieve SO_2 presence below this threshold.

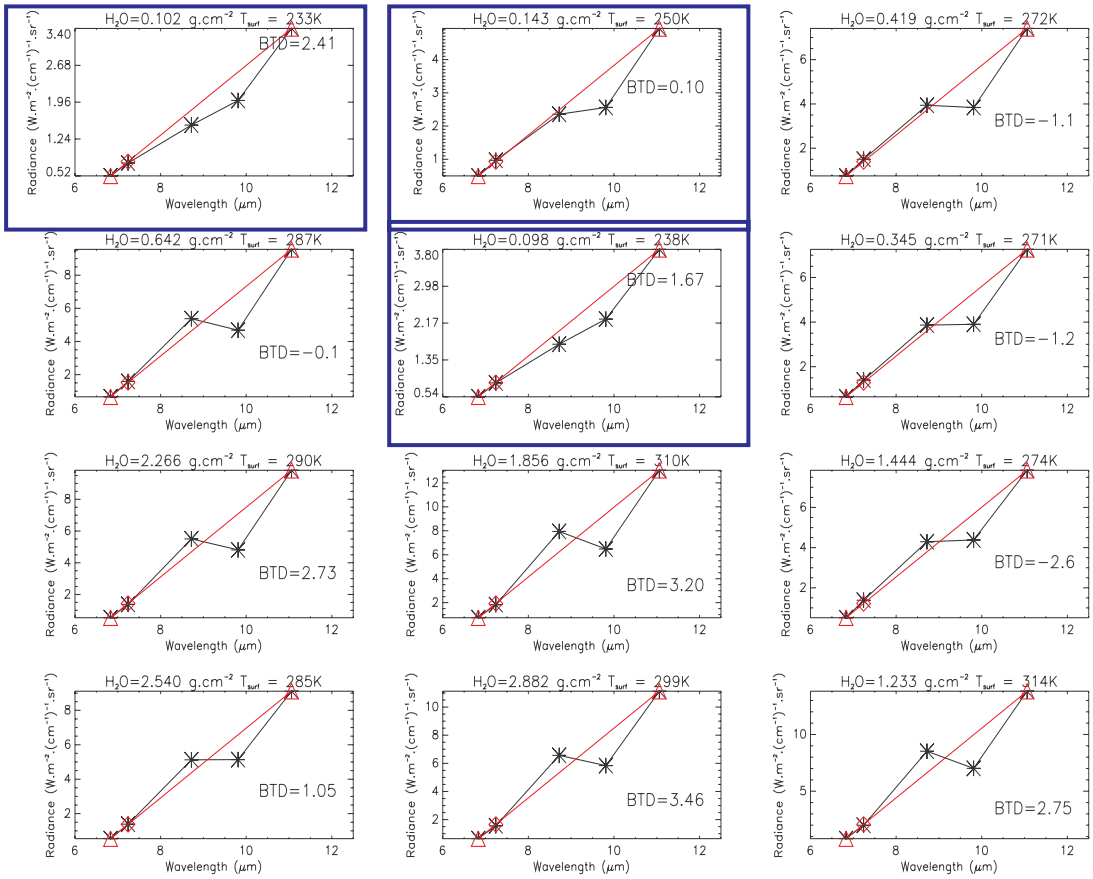

Figure 8: *Simulated MODIS radiances for different bands (27, 28, 29, 30 and 31) using different atmospheric profiles but no SO_2. The integrated WV in g.cm^{-2} and the surface temperature in K are given in the title of each figure. Simulations are done using the LBLDOM code. The red diamond shows the linearly interpolated radiance. The resulting brightness temperature difference is given in K for each plot.*

The London VAAC is responsible for the Icelandic region. In this region, even during the summer, the atmospheric water vapour content is expected to small. To test the retrieval scheme we did some more SO_2 sensitivity simulations for two extreme atmospheric profiles: a very cold and dry profile (Figure 9) and a very hot and humid one (Figure 10). Four different SO_2 profiles have been used for the simulations. Results show that the SO_2 plume needs to be high enough in the atmosphere to induce positive values of the difference between the linearly interpolated radiances at 7.3 µm and the observed radiance.

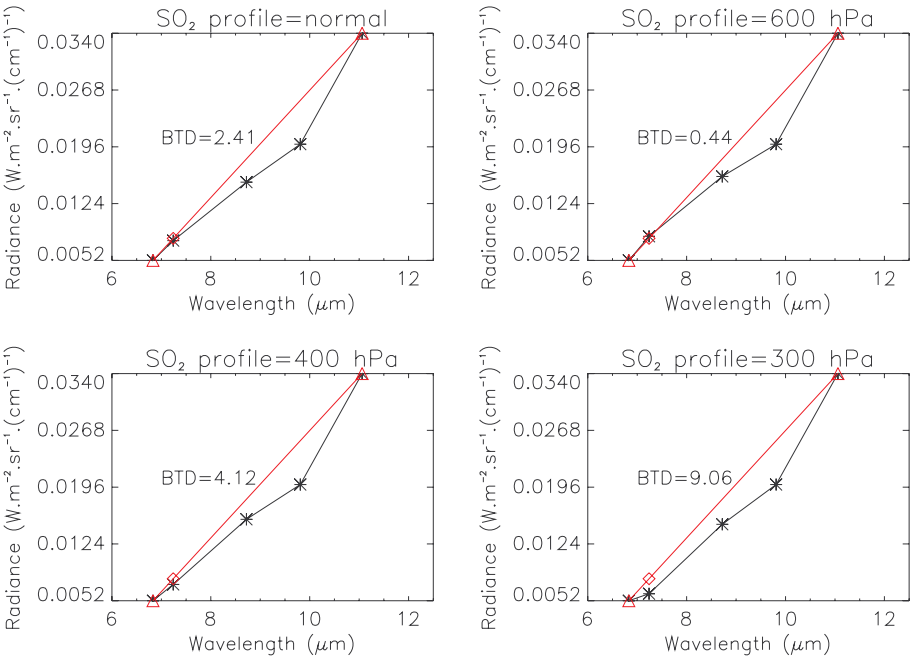

Figure 9: *LBLDOM simulation of radiance at the top of the atmosphere using a cold and dry profile (**H_2O = 0.102 g.cm^{-2}, T_{surf} = 233.85 K**). For each profile four different SO_2 profiles are used. The SO_2 profile labelled "normal" represents a default SO_2 profile (total SO_2 column content of 0.1DU), the three others represent SO_2 profiles representative of a volcanic eruption. The resulting brightness temperature difference is given in K.*

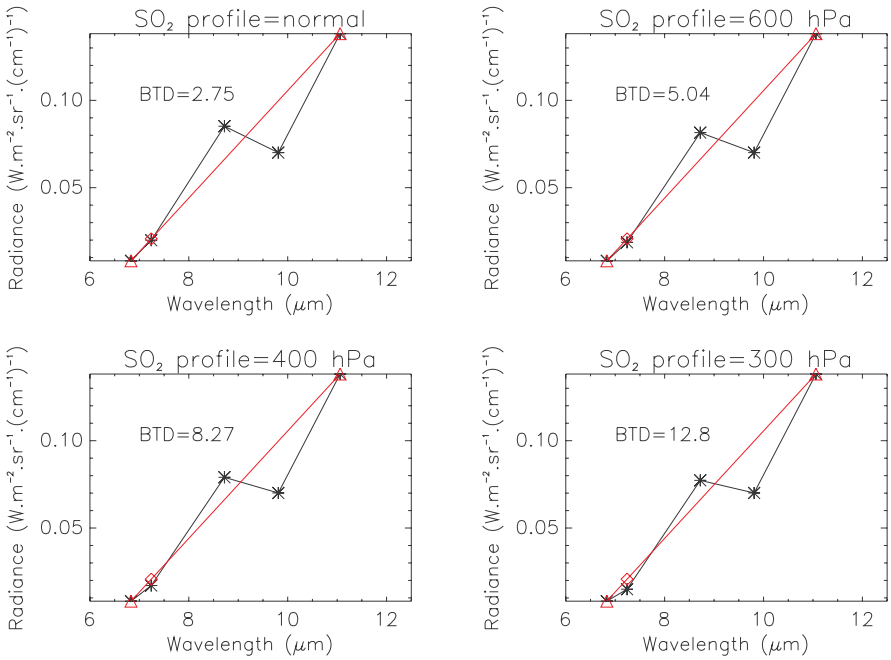

Figure 10: *same as Figure 9 but LBLDOM simulations are done using a hot and humid atmospheric profile (**H_2O = 1.233 g.cm^{-2}, T_{surf} = 314.16 K**) profile.*

4.2.2 Impact of cirrus clouds on the retrieval algorithm

One of the major problems in the detection of SO_2 is the presence of clouds. Low level cloud will have no importance but high level clouds like cirrus will have a critical impact. Further simulations using the same LBLDOM model have been performed. We used a

standard atmospheric profile including a cirrus cloud located at the tropopause (temperature between 223 and 216 K) with four different optical thicknesses. The influence of cirrus clouds on the SO_2 detection is summarised in Table 5 and Figure 11. When a cirrus cloud is present in the column, the estimated brightness temperature is, as for SO_2, larger than the observed BT at 7.3 µm. This variation is not only due to the change in 7.3 µm but also to the decrease in radiances at 6.8 and 10.8 µm used for the interpolation. The effect of cirrus clouds on this 3-channel algorithm is therefore comparable to the SO_2 effect. Other channels (such as MODIS channel 30 or MSG channel 8) should be used to discriminate between cirrus clouds and SO_2 presence.

	Cirrus τ	MODIS 28	MODIS29	MODIS30	MSG 7.3	MSG 8.7
	No	252.98	284.65	270.36	253.56	284.89
	0.1	251.99	283.10	269.28	252.56	283.33
model	0.2	250.99	281.49	268.15	251.54	281.71
Profile 6	0.5	248.10	276.68	264.75	248.61	276.87
US	1	243.76	269.26	259.57	244.20	269.39

Table 5: *Brightness temperature (K) simulated with LBLDOM model for an atmospheric profile containing a cirrus located at the tropopause (between 223 and 216 K) in different MODIS and MSG channels.*

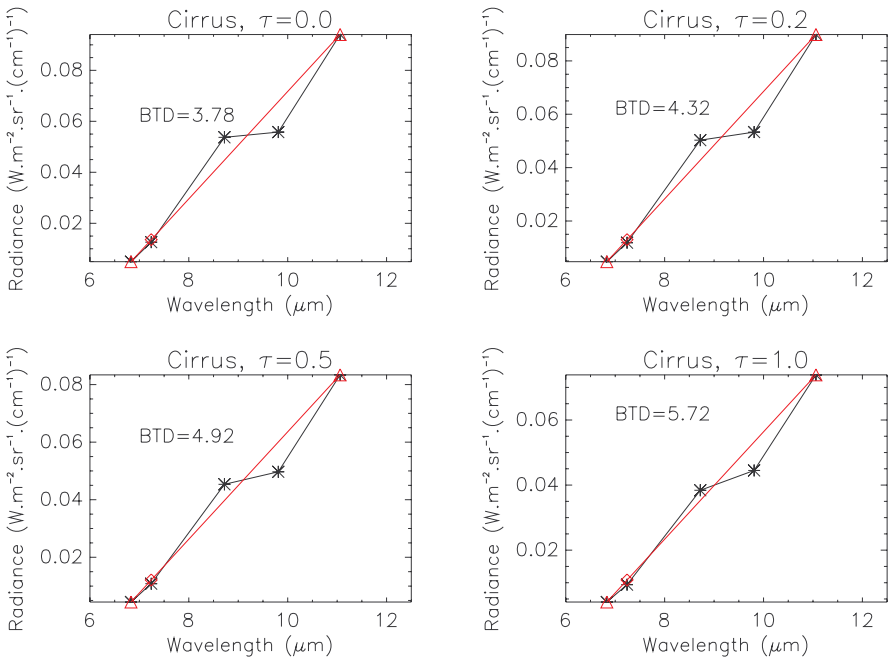

Figure 11: *LBLDOM simulation of radiance at the top of the atmosphere using a summer artic profile. The cirrus is located around 10 km above the surface. For each profile four different cirrus optical thickness are used. The resulting brightness temperature difference is given in Kelvin.*

Alternatively one can look at ratio of radiances to discriminate between cirrus and SO_2. Table 6 indicates how radiances in different wavelengths vary as a function of the cirrus optical thickness and SO_2 profile. We show that the R27/R28 and R28/R31 ratios are relatively insensitive to cirrus clouds. Large (resp. small) values of the R27/R28 (resp. R28/R31) ratios may therefore be indicative of SO_2 presence.

τ wavelength	0	0.2	0.5	1
6.83	4.944	4.743	4.462	4.066
7.24	12.605	11.856	10.823	9.399
11.06	94.036	89.884	83.366	73.859
R27/R28	0.392	0.400	0.412	0.412
R28/R31	0.134	0.132	0.130	0.127
BTD at 7.3	3.783	4.320	4.923	5.728

SO_2 wavelength	No SO_2	600hPa	400hPa	300hPa
6.83	4.944	4.944	4.944	4.944
7.24	12.605	10.778	9.323	8.014
11.06	94.036	94.036	94.036	94.036
R27/R28	0.394	0.457	0.529	0.617
R28/R31	0.139	0.120	0.103	0.089
BTD at 7.3	3.783	8.791	13.253	17.743

Table 6: *Radiance values for different wavelengths obtained for different cirrus optical thicknesses and different SO_2 altitude.*

5. Case studies from MODIS measurements

5.1 Brief description of the different volcanoes

Volcanoes used here are mainly those chosen by Watkin (2005). Figure 12 shows the geographical location of the different volcanoes used in this study.

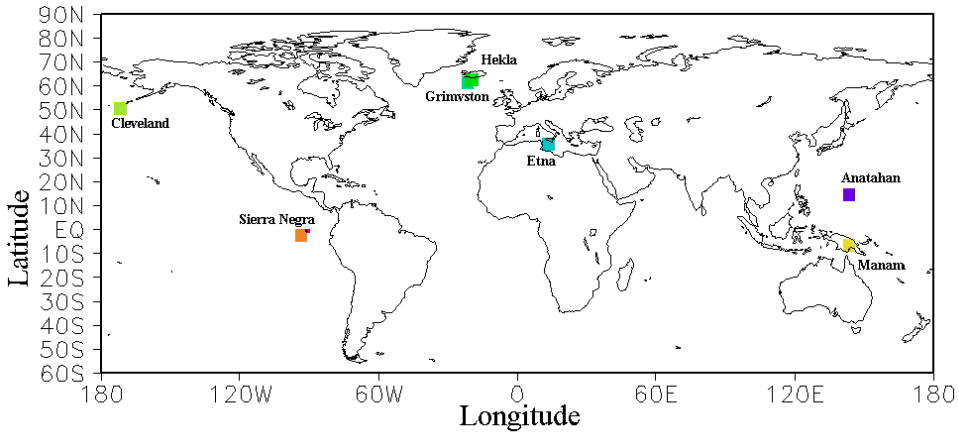

Figure 12: *Location of the eight different volcanoes used in this study.*

Table 7 shows the time and date of the MODIS data used in this study.

Volcano	*Location*		*Date and time of the imagery*	*MODIS satellite used*
	Latitude	*Longitude*		
Hekla	63.97	-19.7	28/02/2000 11:15	Terra
Cleveland	52.82	-169.94	19/02/2001 23:10	Terra
Etna	37.73	15.00	28/10/2002 12:15	Aqua
Anatahan	16.35	145.67	11/05/2003 01:25	Terra
Grimsvotn	64.42	-17.33	02/11/2004 12:10	Terra
Manam	-4.10	145.06	25/01/2005 03:55	Aqua
Sierra Negra	-0.83	-91.18	23/10/2005 16:20	Terra

Table 7: *List of the MODIS granules used for each of the volcanic eruption.*

Grimsvotn and Mount Hekla are located in Iceland. Mount Hekla is one the Iceland's most prominent and active volcanoes. Late in the evening of Monday 1 November 2004 the Grimsvotn volcano on Iceland erupted spectacularly. The eruption of Grimsvotn emitted not just ash and water vapour into the atmosphere, but also other gases such as SO_2. The SCIAMACHY (SCanning Imaging Absorption SpectroMeter for Atmospheric CHartographY, SCHIAMACHY) instrument, aboard ENVISAT (Environmental Satellite) of the European Space Agency (ESA), measured SO_2 concentrations well above the normal background level when the satellite passed over Iceland around 12:14 UTC on 2 November (see Figure 22). Hekla's first historical eruption in 1104 was one of the largest in Iceland's recorded. The Hekla February eruption is the first explosive event studied with the MODIS instrument (Rose et al., 2003). The Cleveland volcano is situated in Alaska at 52º49'N, 169º57'W, 1500 km southwest of Anchorage. It had volcanic eruptions on February 19, March 11, and March 19, 2001. Gu et al. (2005) show volcanic ash detection of this volcano using MODIS, AVHRR and GOES instruments. Manam volcano is located northeast of New Guinea. It is monitored by the Darwin VAAC. On 28 January 2005, OMI saw a large cloud of sulphur dioxide drifting west over the island of New Guinea. Sierra Negra is located in the Galapagos Islands. On October 22, 2005, Sierra Negra began erupting. The Sierra Negra Volcano continued to emit ash clouds and lava through the end of the month, before apparently settling down around October 31. The volcanic emissions contained sulphur dioxide gas as shown by the OMI instrument.

5.2 Results

The results for the different eruptions are presented graphically in Appendix 1, Figure 22. The algorithm used over many different eruptions shows that the difference between the estimated and observed 7.3 µm brightness temperature is always positive. In some cases an SO_2 plume is clearly visible, in some cases this is not the case and the product can be noisy. We further examine this by showing on Figure 13 scatter plots of the linearly estimated and observed 7.3 µm BT for a region around the plume. For eruptions like Anatahan or Grimvston, the relationship between the estimated and observed 7.3 µm BT is very linear and no strong deviation from the one-to-one line appears. In these cases, the SO_2 detection will be very difficult as SO_2 seems not to be distinguished from the background. For other eruptions, like Hekla or Sierra Negra, a clear pattern appears where the estimated BT is much larger than the observed one. This pattern can then be identified as containing SO_2.

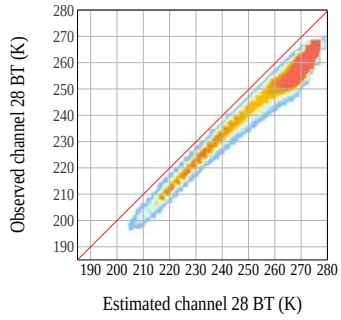

Anatahan eruption

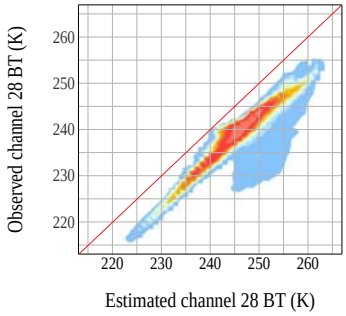

Hekla eruption

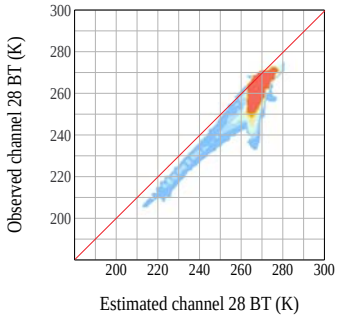

Sierra Negra eruption

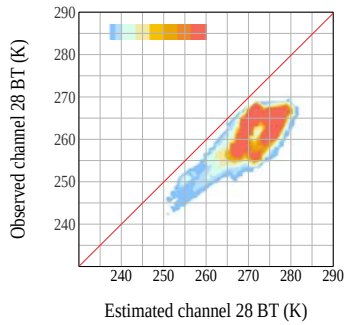

Etna eruption

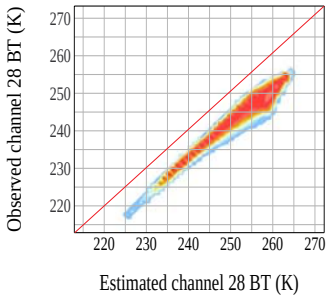

Cleveland eruption

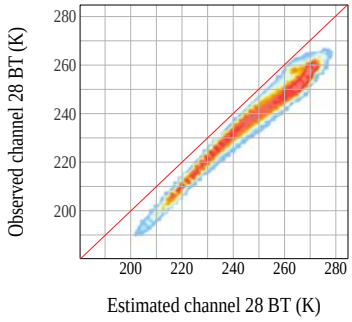

Grimsvotn eruption

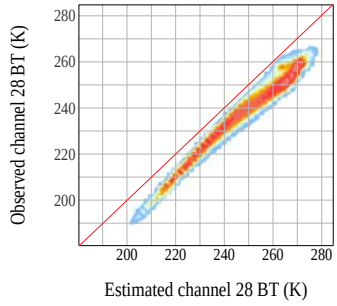

Manam eruption

Figure 13: *Scatter plot of the observed 7.3 µm BT as a function of the linearly estimated one. The red line is the 1:1 line.*

As shown on Figure 14, there are few cases with a very clear high positive BTD. Firstly, Mount Hekla is located in Iceland and the atmosphere was probably very cold and dry, which makes it easier for the SO_2 weight function to peak above the water vapour weight function at 7.3 µm. The SO_2 was also certainly located high enough in the atmosphere to be detected.

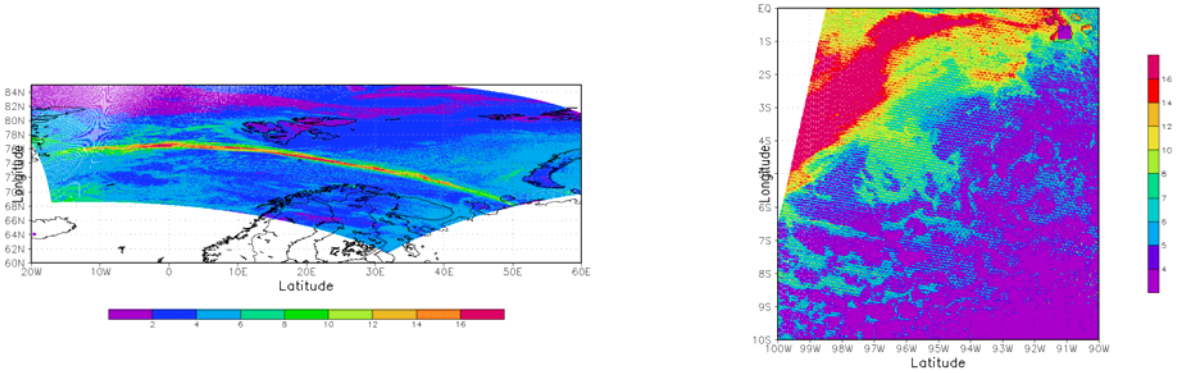

Figure 14: *Two successful retrievals presenting a strong positive 7.3 µm BTD between the linearly estimated and the observed BT. Left: Mount Hekla eruption Right: Sierra Negra eruption.*

The second case of a good retrieval is the eruption of the Sierra Negra volcano in the Galapagos Islands. For both of these examples, there is no or very little presence of ash. Ash affects the 10.8 µm channel as it absorbs at this wavelength. This absorption feature is used in the "split window" IR retrieval technique employed to detect volcanic ash (Prata, 1989; Yu and Rose, 2002; Watkins, 2005). Example of unsuccessful cases such as the Anatahan eruption (Figure 22) shows quite a large volcanic ash content (negative yellowish colours on the plots). When the SO_2 plume follows the ash plume, it is indeed much more difficult to detect it. A second reason that could explain the good detection of SO_2 during the Sierra Negra eruption could also be that the SO_2 was located very high in the atmosphere.

The 7.3 µm BTD is usually larger when SO_2 is present, so a possibility to identify the SO_2 presence would be to display only BTD when it is larger than the BTD average in a certain geographical area around the volcano (hot spot detection technique). Such a product is shown in Figure 15. Another useful plot is shown in Figure 16 where we only plot the BTD when the R27/R28 ratio is larger than the average value over the region. R27/R28 ratios are also presented in Figure 22.

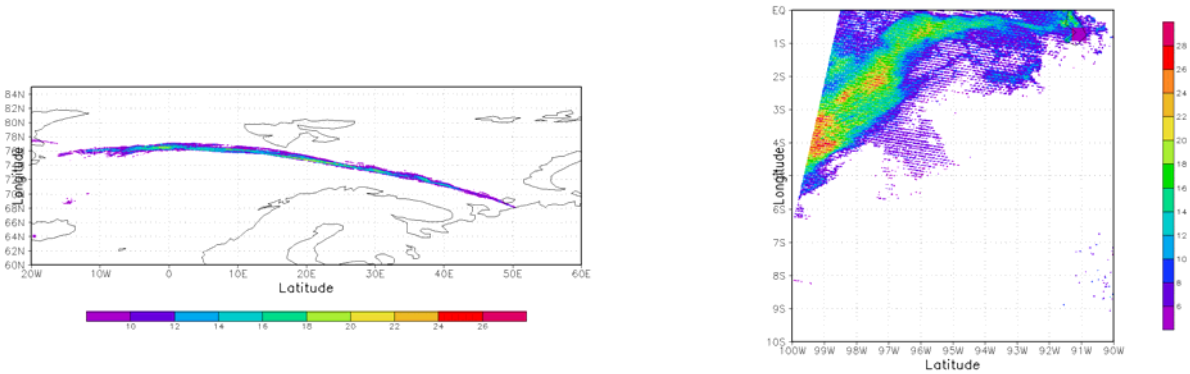

Hekla eruption, average BTD = 4.2K *Sierra Negra eruption, average BTD = 2.9K*

Figure 15: *7.3 µm BTD (linearly estimated – observed), values are plotted only when the difference is twice larger than the average BTD in the geographical area.*

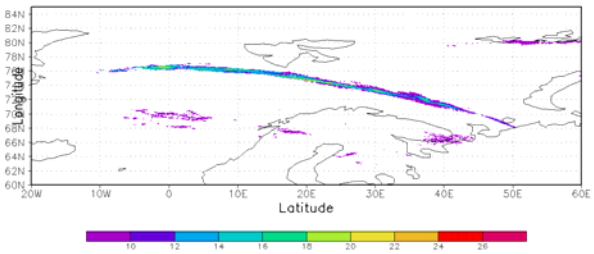

Hekla eruption, average ratio = 0.48

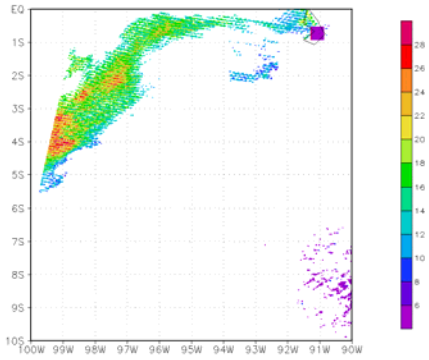

Sierra Negra eruption, average ratio = 0.36

Figure 16: *7.3 µm BTD (linearly estimated – observed), values are plotted only when the ratio of radiances in channels 27 and 28 is larger than the ratio average by 20% of the average ratio in the geographical area.*

6. Possible exploitation of SEVIRI

There has been only one major volcanic eruption in the Meteosat disc since the launch of MSG-1, thus offering little opportunity for testing the retrieval technique applied to the SEVIRI instrument. As the MODIS and SEVIRI channels are not quite the same, we first did some comparison between MODIS and SEVIRI for “clear” cases. We chose a MODIS granule over North West Africa and collocated it with the corresponding SEVIRI image.

6.1 Comparison of MODIS and SEVIRI channels

Figure 17 and Figure 18 show the MODIS and SEVIRI radiances and brightness temperatures, respectively, for the three channels used in our retrieval. There is a good agreement for radiances and brightness temperatures around 7.3 and 10.8 µm. The SEVIRI channel closest to the MODIS channel 27 at 6.8 µm is channel 5 at 6.2 µm, which is located outside the range of wavelengths where the radiance can be considered roughly linear. As a result, using SEVIRI channel 5 (6.2 µm) in the algorithm to interpolate the brightness temperature at 7.3 µm leads to rather large values for the brightness temperature difference, which would make it difficult to distinguish an SO_2 signal from the large background values. There are two options to circumvent this problem. We can either use the ratio of radiances between 6.2 and 7.3 µm as a measure of the SO_2 content or extrapolate the radiance in the 6.2 µm channel to a virtual 6.8 µm channel (assuming a blackbody) and apply our algorithmfor MODIS as it is.
Figure 19 shows that these two options produced similar patterns for the SEVIRI and MODIS data, which gives some confidence that the presence of SO_2 would show up in the SEVIRI images as well.

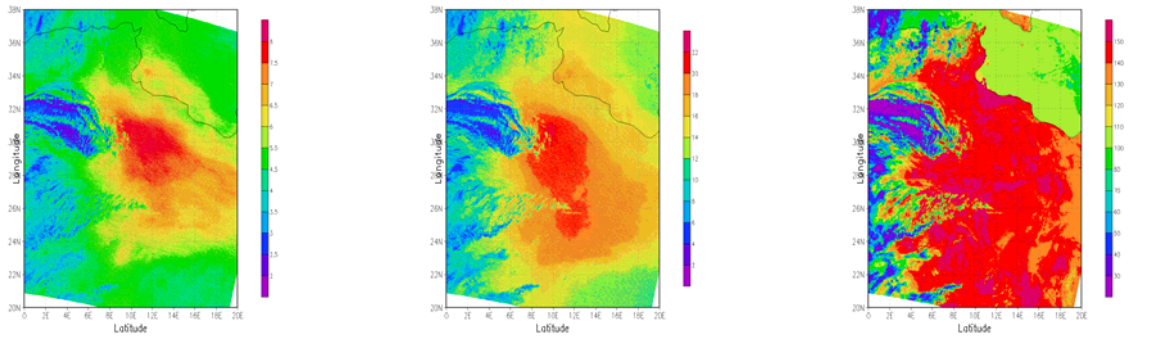

a) Radiance 6.8 µm MODIS *b) Radiance 7.3 µm MODIS* *c) Radiance 10.8 µm MODIS*

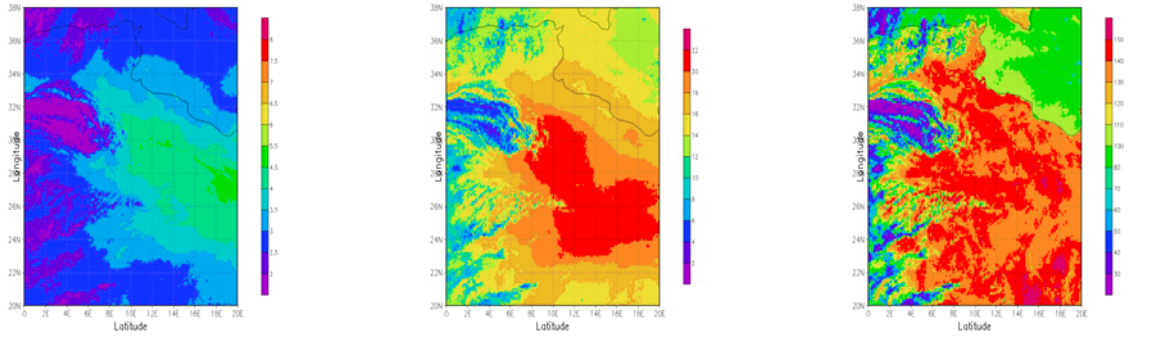

d) Radiance 6.2 µm SEVIRI *e) Radiance 7.3 µm SEVIRI* *f) Radiance 10.8 µm SEVIRI*

Figure 17: *Radiances ($mW.m^{-2}.sr^{-1}.(cm^{-1})^{-1}$) observed by MODIS and SEVIRI on 22 May 2006 at 10:00 (SEVIRI) and 10:05 (MODIS Terra) over NW Africa.*

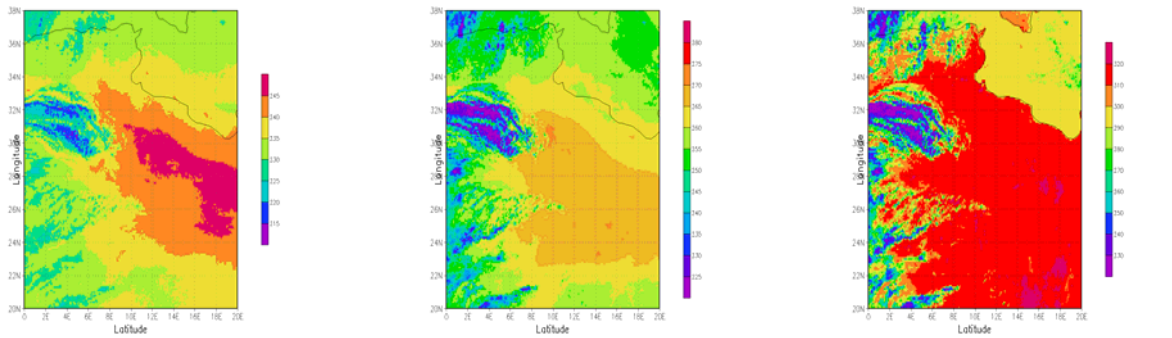

a) BT at 6.2 µm SEVIRI (in K) *b) BT at 7.3 µm SEVIRI (in K)* *c) BT at 10.8 µm SEVIRI (in K)*

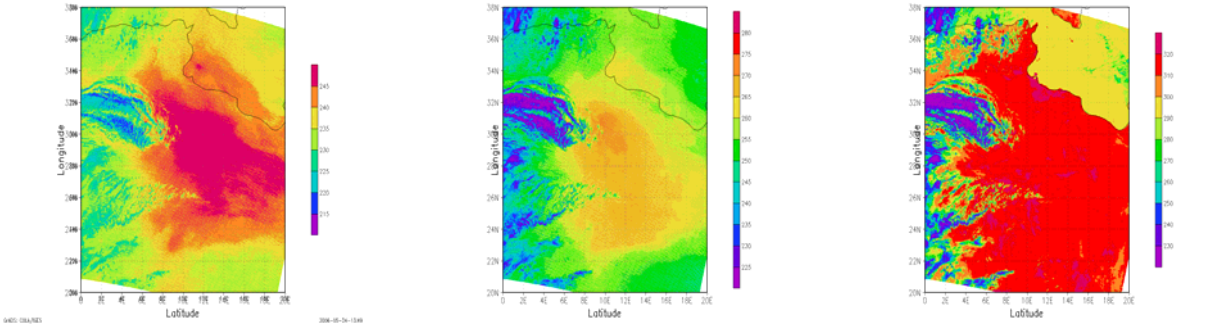

d) BT at 6.8 µm MODIS *e) BT at 7.3 µm MODIS* *f) BT at 10.8 µm MODIS*

Figure 18: *Brightness temperatures (K) observed by MODIS and SEVIRI on 22 May 2006 at 10:00 (SEVIRI) and 10:05 (MODIS Terra).*

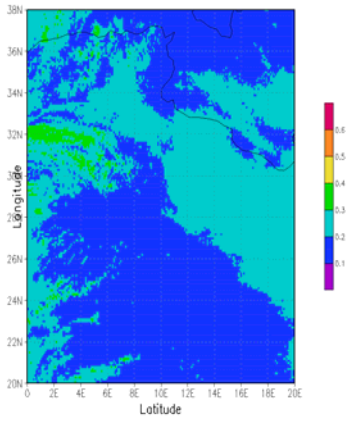

a) Radiance 6.2 µm / Radiance 7.3 µm SEVIRI (average= 0.2)

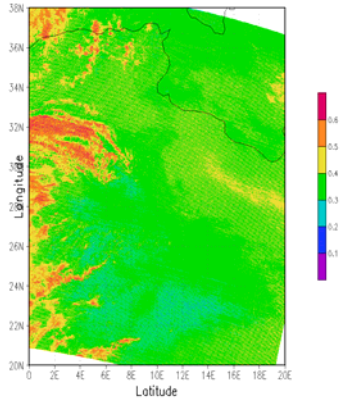

b) Radiance 6.8 µm / Radiance 7.3 µm MODIS (average= 0.38)

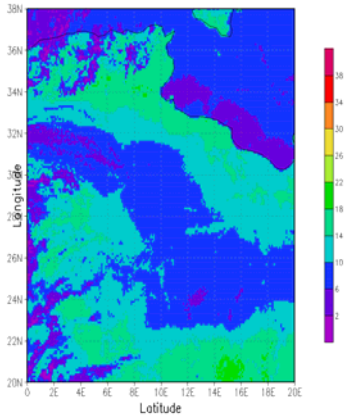

c) Difference between the estimated and observed BT at 7.3µm BT for SEVIRI (but extrapolating the 6.2 µm channel to 6.8µm).

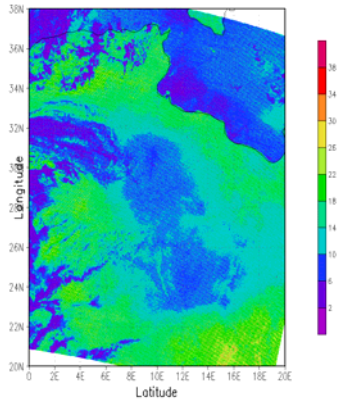

d) Difference between the estimated and observed BT at 7.3µm for MODIS.

Figure 19: ***First row:*** *Radiance ratios for SEVIRI and MODIS,* ***second row:*** *brightness temperature difference obtained at 7.3 µm for SEVIRI and MODIS.*

6.2 Example of SEVIRI retrieval

Soufriere Hills volcano, on the island of Montserrat (16.7 N, 62.2 W, 2000 m) in the Caribbean Sea has been in a state of eruption since 1995. On the morning of 20 May 2006, after several months of growing lava dome, the eastern flank of the volcano suffered a major collapse with an estimated volume of 90 million m^3 of lava, much of it flowing into the ocean. The eruption caused a column of ash and gas to rise to heights of at least 17 km and the gases penetrated the tropopause and entered the stratosphere, reaching as high as 20 km. The initial phase of the eruption was not captured well by the polar orbiting satellite instruments due to mismatch between the timing of the satellite passes and the onset of the eruption. However, MSG SEVIRI was able to monitor the eruption[1] cloud within 15 minutes of the eruption. We tested our algorithm on this case. Difference between the

[1] http://oiswww.eumetsat.org/WEBOPS/iotm/iotm/20060521_montserrat/20060521_montserrat.html#pics

estimated BT and the observed one are shown on Figure 20. The ratio of 6.8 over 7.3 µm is also presented on this Figure. As for MODIS retrieval we show that there is a correlation between these two parameters.

a) BTD in K

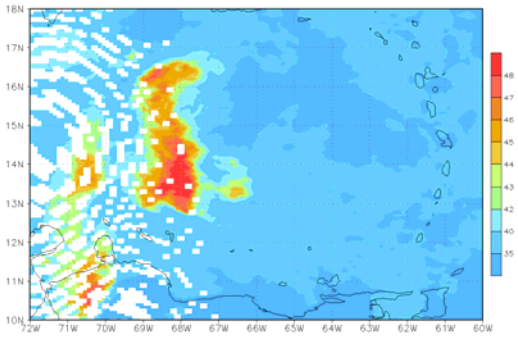

b) Ratio R6.8/R7.3

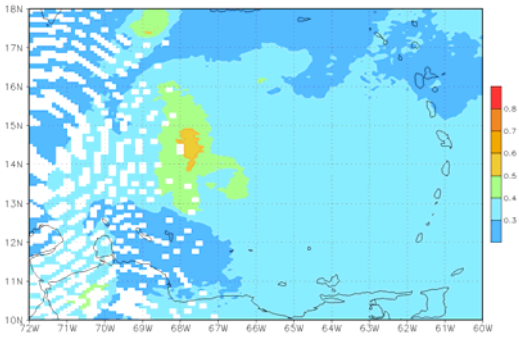

Figure 20*: 21 May 2006, 2:15 UTC Montserrat eruption.*

We retrieve the BTD for pixels having a ratio higher than the average by 20%. Results are shown on Figure 21. We see the SO_2 cloud moving to the West part of the image. This retrieval gives us confidence that the algorithm will work when implemented in operations.

a) 20 May 2006, 22:15 UTC

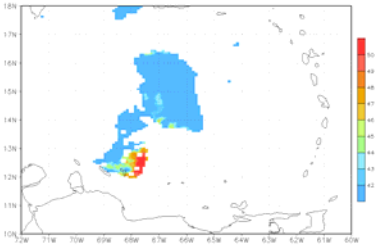

b) 20 May 2006, 22:45 UTC

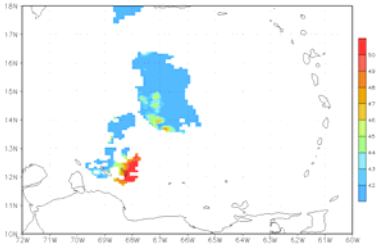

c) 20 May 2006, 23:15 UTC

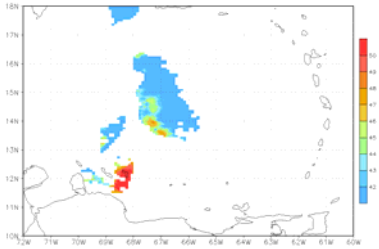

d) 20 May 2006, 23:45 UTC

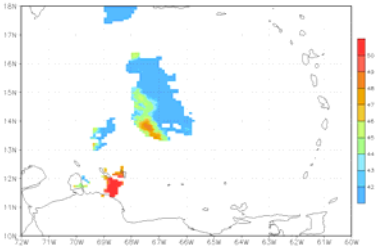

e) 21 May 2006, 00:15 UTC

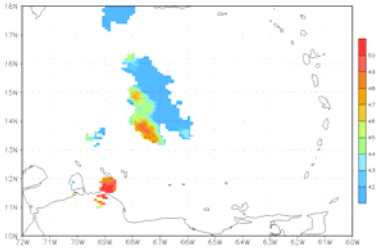

f) 21 May 2006, 00:45 UTC

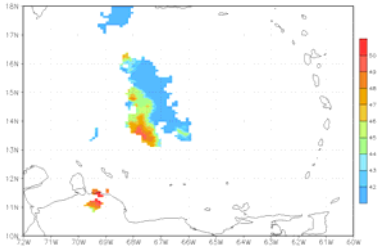

g) 21 May 2006, 1:15 UTC

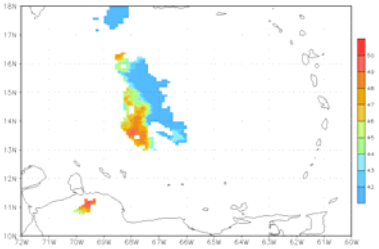

h) 21 May 2006, 1:45 UTC

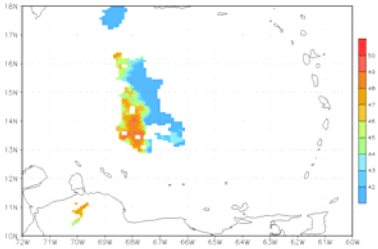

i) 21 May 2006, 2:15 UTC

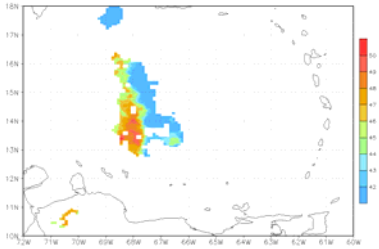

j) 21 May 2006, 2:45 UTC *k) 21 May 2006, 3:15 UTC* *l) 21 May 2006, 3:45 UTC*

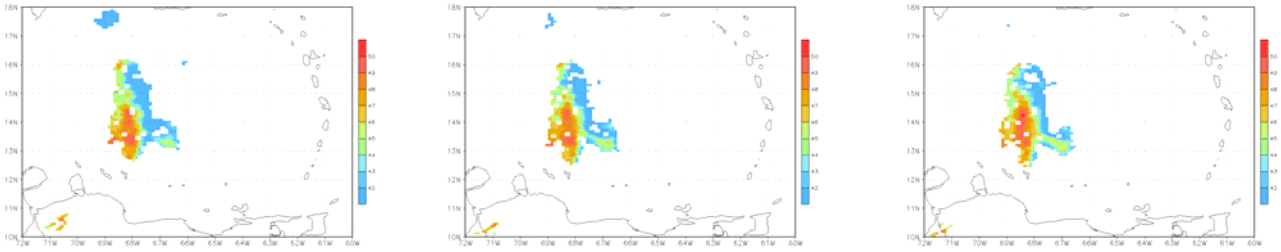

Figure 21: *7.3 μm BTD (linearly estimated – observed), values are plotted only when the ratio of radiances at 6.8 and 7.3 μm is larger than the ratio average by 20%.*

7. Conclusions

This study shows the potential to use MODIS and SEVIRI data to detect SO_2 from volcanic eruptions. SO_2 detection from space can be very useful for aviation as SO_2 presence could sometime indicate volcanic ash in the vicinity. Ash is not always detected, so SO_2 can be used as another marker for ash presence.

For this purpose we have chosen to apply the three-channel retrieval algorithm of Prata to MODIS and SEVIRI data. The algorithm could only be tested on one eruption with SEVIRI data because there has been no other volcanic eruption in the MSG disc region since MSG went operational.

The three-channel Prata algorithm has been laid on firmer grounds by *i)* looking at the best way to interpolate radiances between the 6.8 and 10.8 μm channels and *ii)* performing accurate radiative transfer simulations of the 6.8, 7.3 and 10.8 μm radiances with several different SO_2 profiles, under different atmospheric conditions (i.e. varying water vapour content and temperature, presence of cirrus clouds).

It has been demonstrated that for the algorithm to be successful:

- SO_2 should be located high enough in the atmosphere.
- The atmosphere should be cirrus free or some cloud screening technique should be implemented. This is because cirrus clouds have a similar signature as SO_2 on the BT difference at 7.3 μm (although for different physical reasons).
- The atmosphere should have little or no ash. When an SO_2 plume follows the ash plume, it is much more difficult to detect it.

The SO_2 detection scheme has been successfully applied to various case studies. There are nevertheless known eruptive emissions of SO_2 which do not show up in this product as well as cases of contamination by cirrus clouds. We tested simple ways to strengthen the SO_2 signal in the final image product albeit with a limited success. Outputs from this SO_2 detection scheme should therefore be treated cautiously by trained forecasters. We nevertheless expect the SO_2 detection scheme to be useful in combination with other sources of data (presence of cirrus clouds, knowledge of the time and location of the eruptive volcano). The SO_2 detection scheme will help to provide early warning to the civil aviation in case of known volcanic eruptions, especially for cases where the ash detection system failed.

Future SO_2 retrieval schemes could also rely on high spectral resolution instruments such as the Infrared Atmospheric Sounder Interferometer (IASI) on board the polar orbiting satellite METOP. The IASI spectral range (15.5 to 3.62 µm) covers the SO_2 absorption bands. Using IASI, some channels could be selected in the IR SO_2 absorption spectrum where there is no overlapping with other atmospheric constituents. Finally SO_2 products from instrument such as TOMS/OMI or SCHIAMACHY could also be used by the VAAC to help forecasters.

References

Andres, R. J., A. D. Kasgnoc, A time-averaged inventory of subaerial volcanic sulphur emissions, *J. Geophys. Res.*, 103 (D19), 25251-25261, 1998.

Baran, A. J., J. S. Foot, P. C. Dibben, Satellite detection of volcanic sulphuric acid aerosol, *Geophys. Res. Lett*, 20, 1799-1801, 1993.

Carn, S.A., L. L. Strow, S. de Souza-Machado, Y. Edmonds, and S. Hannon, Quantifying tropospheric volcanic emissions with AIRS: the 2002 eruption of Mt Etna (Italy), *Geophys. Res. Lett*, 32, L02301, doi:10.1029/2004GL021034, 2005.

Carn, S. A., A. J. Krueger, N. A. Krotkov, and M. A. Gray, Fire at Iraqi sulphur plants emits SO_2 clouds detected by earth probe TOMS, *Geophys. Res. Lett*, 31, L19105, doi:10.1029/2004GL020719, 2004.

Clough, S. A., F. X. Kneizys, and R. W. Davies, Line shape and the water vapour continuum, *Atmos. Res.*, 23, 229-241, 1989.

Dubuisson P., J. C. Buriez, and Y. Fouquart, High spectral resolution solar radiative transfer in absorbing and scattering media: application to the satellite simulation, *J. Quant. Spectrosc. Radiat. Transfer*, 55, 103-126, 1996.

Dubuisson P., V. Giraud, O. Chomette, H. Chepfer and J. Pelon, Fast Radiative Transfer Modeling for Infrared Imaging Radiometry, *J. Quant. Spectrosc. Rad. Transfer*, 95, 201-220, 2005.

Francis P., M. R.Burton, and C. Oppenheimer, Remote measurements of volcanic gas compositions by solar occultation spectroscopy, *Nature*, 396, 567- 570, 1998.

Gu, Y., W. I. Rose, D. J. Schneider, G. J. S. Bluth and I. M. Watson, Advantageous GOES IR results for ash mapping at high latitudes: Cleveland eruptions 2001, *Geophys. Res. Lett.*, 32: L02305, doi:10.1029/2004GL021651, 2005.

Guo, S., G. J. S. Bluth, W. I. Rose, I.M. Watson, and A. J. Prata, Re-evaluation of SO_2 release of the June 15, 1991 Pinatubo eruption using ultraviolet and infrared satellite sensors, *Geochem. Geophys. Geosystems*, doi:10.1029/2003GC000654, 2004.

Halmer, M. M., H. U. Schmincke, and H. F. Graf, The annual volcanic gas input into the atmosphere, in particular into the stratosphere: a global data set for the past 100 years, *J. Volcano. Geotherm. Res.*, 115, 511-528, 2002.

Krueger, A. J., Sighting of El Chichon sulphur dioxide clouds with the Nimbus 7 Total Ozone Mapping Spectrometer, *Science*, 220, 1377-1378, 1983.

Krueger, A. J., L. S. Walter, P. K. Bhartia, C. C. Schneltzler, N. A. Krotkov, I. Sprod, and G.J.S. Bluth, Volcanic sulphur dioxide measurements from the total ozone mapping spectrometer instruments, *J. Geophys. Res.*, 100, D7, 14057-14076, 1995.

Lacis, A., J. Hansen, M. Sato, Climate forcing by stratospheric aerosols, *Geophys. Res. Lett.*, 19, 1607-1610, 1992.

Prata A. J., Observations of volcanic ash clouds in the 10-12 μm window using AVHRR/2 data, *Int. Remote Sensing*, 10, 751-761, 1989.

Prata, A. J., W. I. Rose, S. Self, and D. M. O'Brien, Global, long-term sulphur dioxide measurements from TOVS data: a new tool for studying explosive volcanism and climate, *AGU Geophysical Monograph 139: Volcanism and the Earth's Atmosphere, edited by A. Robock and C. Oppenhaimer*, pp. 75-92, 2003.

Pugnaghi, S., G. Gangale, S. Corradini, M. F. Buongiorno, Mt. Etna sulfur dioxide flux monitoring using ASTER-TIR data and atmospheric observations, *Journal of Volcanology and Geothermal Research*, doi:10.1016/j.jvolgeores.2005.10.004 , 2006.

Realmuto, V. J., M. J. Abrams. M. F. Buongiorno, and D. C. Pieri, The use of multispectral thermal infrared data to estimate the sulphur dioxide flux from volcanoes: A case study from Mount Etna, Sicily, July 29, 1986, *J. Geophys. Res*., 99 (B1), 481-488, 1994.

Realmuto, V. J., A. J. Sutton, and T. Elias, Multispectral thermal infrared mapping of sulphur dioxide plumes: A case study from the East Rift Zone of Kilauea Volcano, Hawaii, *J. Geophys. Res*., 102 (B7), 15057-15072, 1997.

Realmuto, V. J. and H. W. Worden, Impact of atmospheric water vapour on the thermal infrared remote sensing of volcanic sulphur dioxide emissions: A case study from Pu'u 'O'o vent of Kilauea Volcano, Hawaii, *J. Geophys. Res*., 105 (B9), 21497-21508, 2000.

Rodriguez, L.A., I. M. Watson, W. I. Rose, Y. K. Branan, G. J. S. Bluth, G. Chigna, O. Matias, D. Escobar, S.A. Carn, and T. Fischer, SO_2 emissions to the atmosphere from active volcanoes in Guatemala and El Salvador, 1999-2002, *Journal of Volcanology and Geothermal Research*, 138 (3-4), 345-364, 2004.

Rose, W. I., G. J. S. Bluth and G. G. J. Ernst, Integrating retrievals of volcanic cloud characteristics from satellite remote sensors-a summary, *Philosophical Transactions of Royal Society*, Series A, 358, 1585-1606, 2000.

Rose, W. I., Y. Gu, I. M. Watson, T. Yu, G. J. S. Bluth, A. J. Prata, A. J. Krueger, N. Krotkov, S. Carn, M. D. Fromm, D. E. Hunton, G. G. J. Ernst, A. A. Viggiano, T. M. Miller, J. O. Ballentin, J. M. Reeves, J. C. Wilson, B. E. Anderson, D. Flittner, The February-March 2000 eruption of Hekla, Iceland from a satellite perspective, *AGU Geophysical Monograph 139: Volcanism and the Earth's Atmosphere, ed by A. Robock and C. Oppenheimer*, pp. 107-132. ISBN 0-87590-998-1, 2003.

Rothman L. S., et al., The HITRAN 2004 Molecular Spectroscopic Database, *J. Quant. Spectrosc. Rad. Transfer*, 96, 139-204, 2005.

Schreiner A. J., T. J. Smith, G. P. Ellrod, and F. Prata, Can upper-level SO_2 be monitored using the GOES sounder? *Proceeding of the 13th AMS Conference on Satellite Meteorology and Oceanography*, Norfolk, September 2004.

Stamnes K., S. C. Tsay, W. Wiscombe, and K. Jayaweera, Numerically stable algorithm for discrete-ordinate-method radiative transfer in multiple scattering and emitting layered media, *Appl. Opt.*, 27, 2502, 1988.

Watkin S., Exploitation of Meteosat Second Generation data for volcanic ash monitoring, *Met Office NWP technical report* n°463, 2005.

Watson, I.M., V.J. Realmuto, W.I. Rose, A.J. Prata, G.J.S. Bluth, Y. Gu, C.E. Bader, and T. Yu, Thermal infrared remote sensing of volcanic emissions using the moderate resolution imaging spectroradiometer, *J. Volcanology and Geothermal Research*, 135, 75-89, 2004.

Weibring, P., H. Edner, S. Svanberg, G. Cecchi, L. Pantani, R. Ferrara, and T. Caltabiano, Monitoring of volcanic sulfur dioxide emissions using differential absorption lidar (DIAL), differential optical absorption spectroscopy (DOAS), and correlation spectroscopy (COSPEC), *Appl. Phys., B Lasers Opt.*, 67, 1-8, 1998.

Yu T. and W. I. Rose, Atmospheric correction for satellite-based volcanic ash mapping and retrievals using “split window” IR data from GOES and AVHRR, *J. Geophys. Res*., 107 (D16), doi:10.1029/2001JD000706, 2002.

Appendix 1: SO_2 detection figures

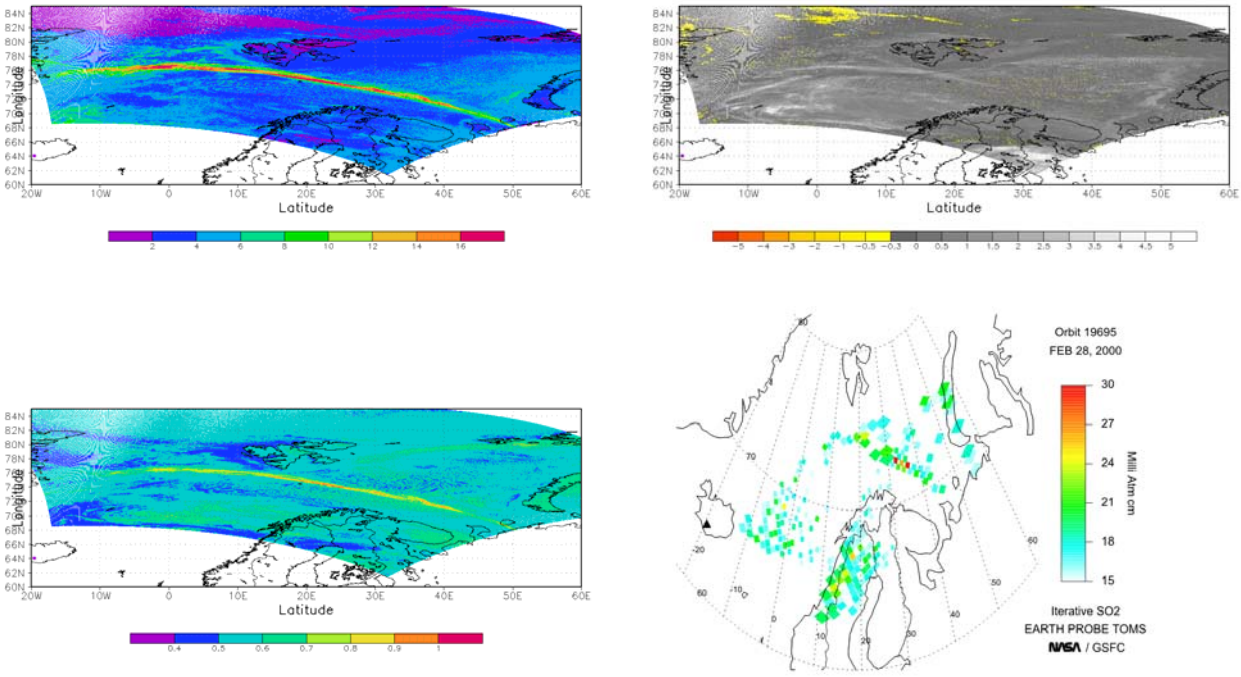

Mount Hekla eruption on 28 February 2000, MODIS Terra data, 11:15UTC.

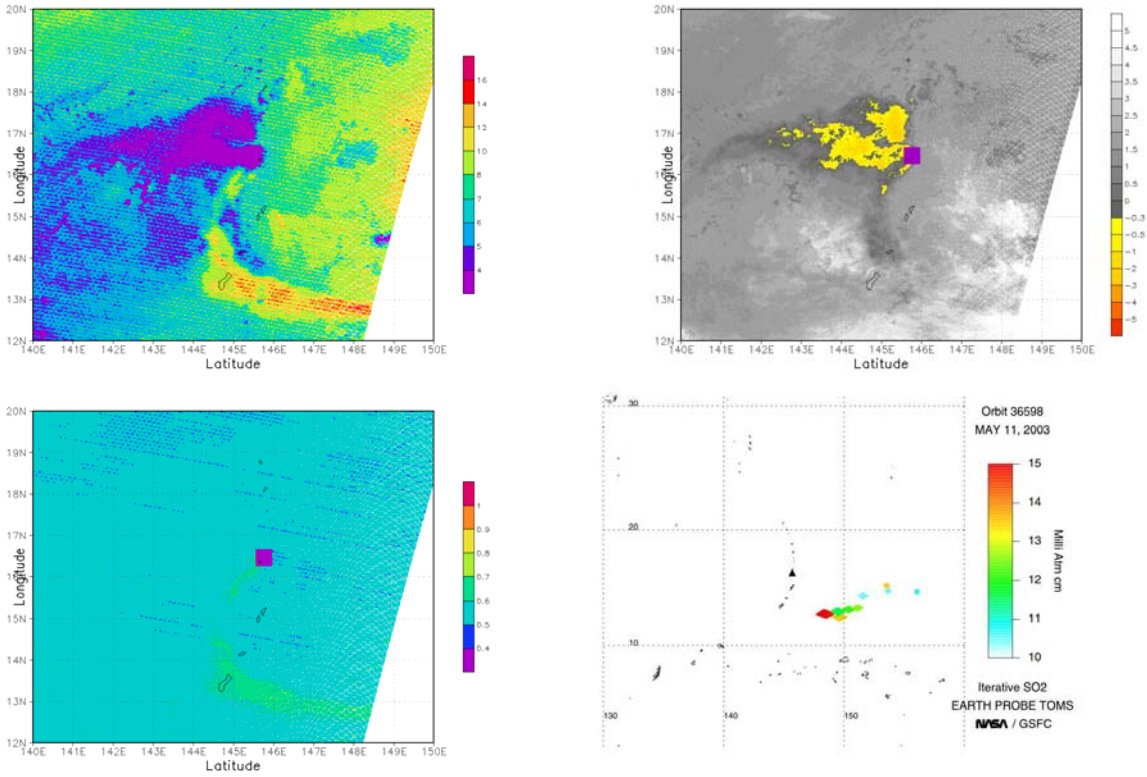

Anatahan eruption on 11 May 2003, MODIS Terra data, 01:25 UTC.

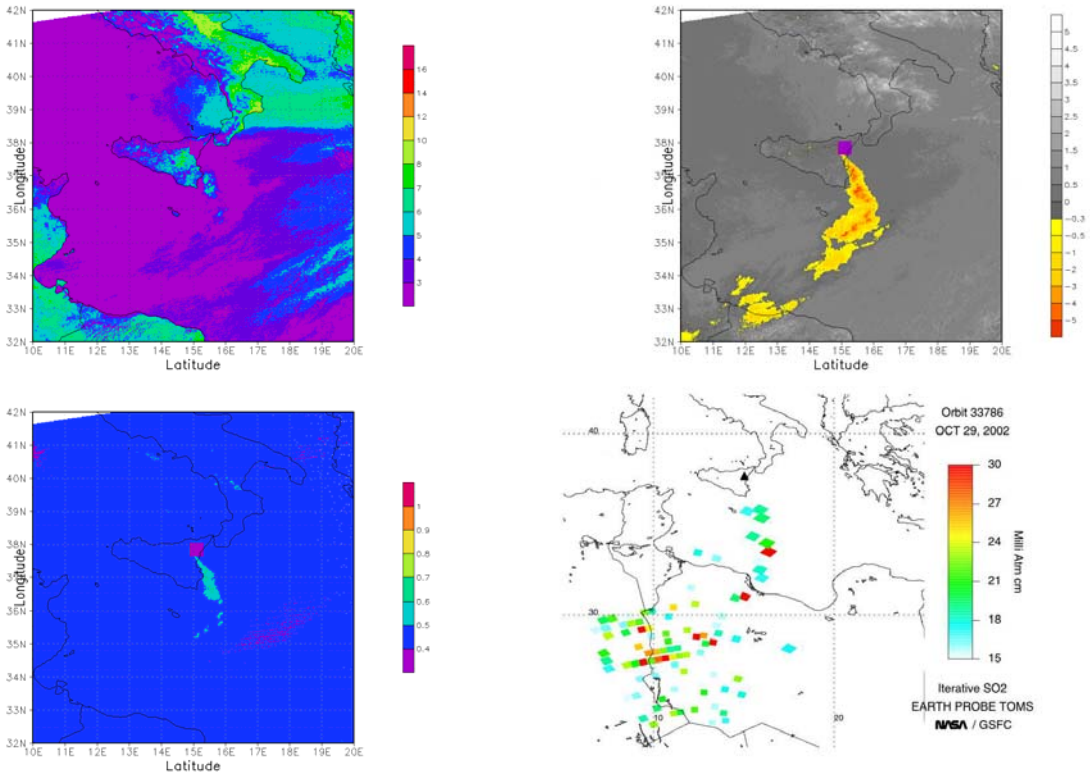

Etna eruption on 28 October 2002, MODIS Aqua data, 12:15UTC.

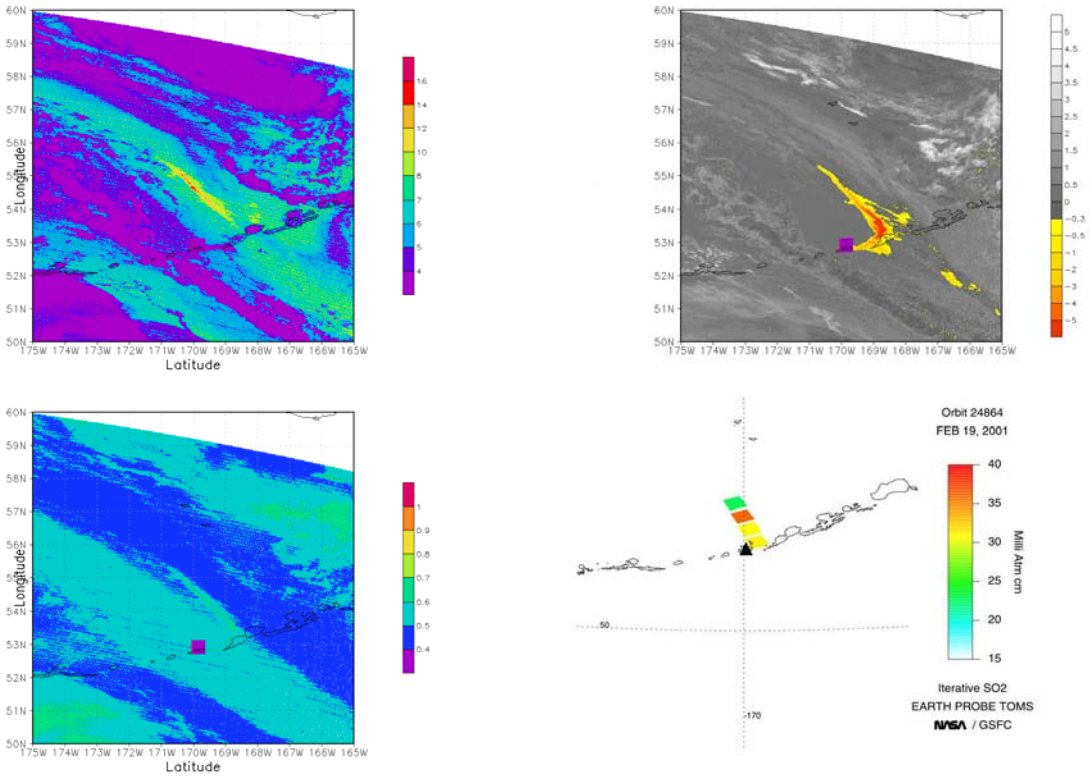

Cleveland eruption on 19 February 2001, MODIS Terra data, 23:10UTC.

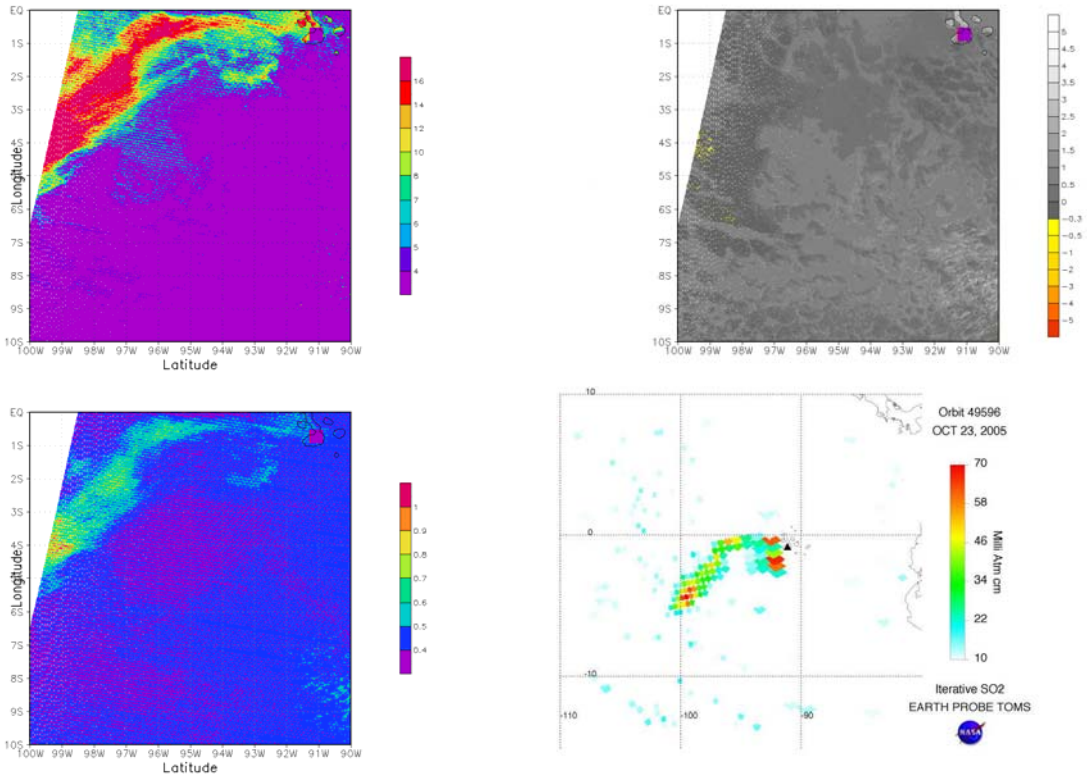

Sierra Negra on eruption, 23 October 2005, MODIS Terra data,16:20UTC.

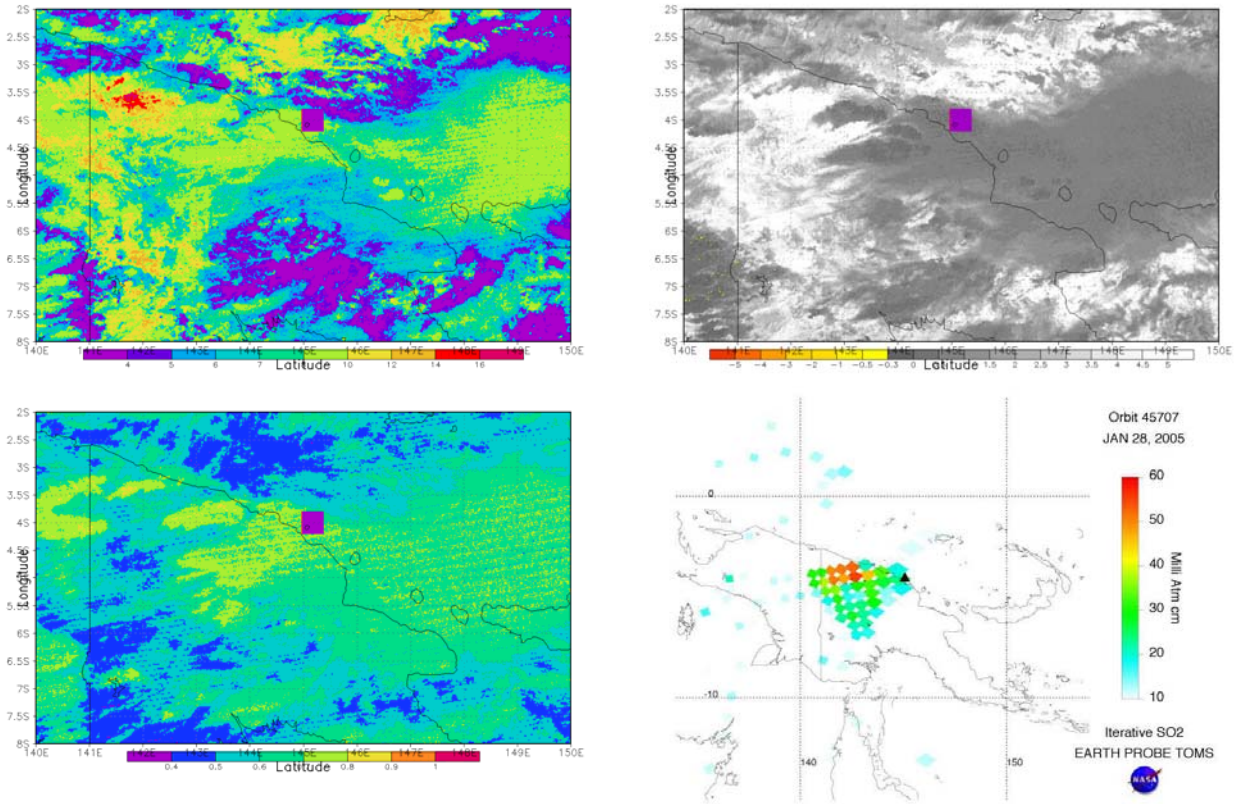

Manam eruption on 28 January 2005, MODIS Aqua data, 3:55UTC.

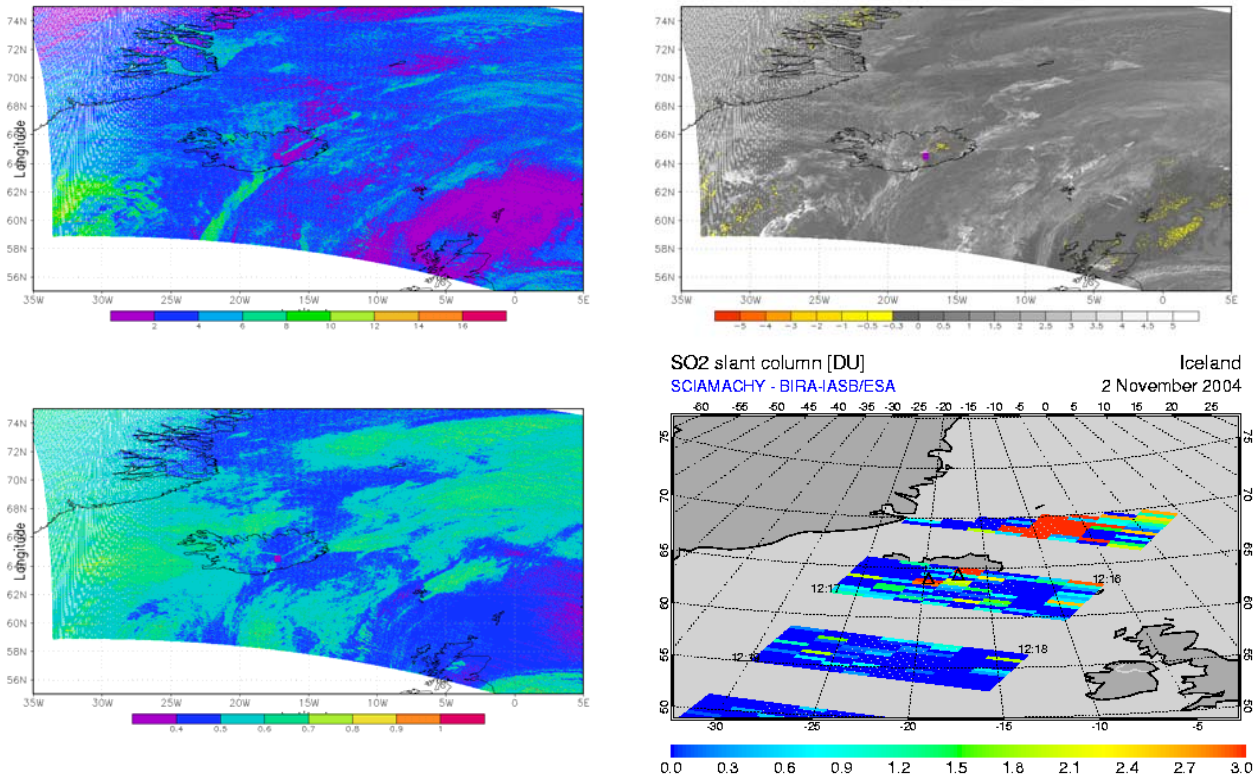

Grimvston eruption on 2 November 2004, MODIS Terra data, 12:10UTC.

Figure 22: *Results of SO_2 detection for different volcanic eruptions using MODIS Aqua and Terra data.* ***First line****: Figures on the left hand side show the 7.3 µm BTD (linearly interpolated – observed) in Kelvin, reddish colours indicate in some cases the presence of SO_2, figures on the right hand side show the 10.8 - 12 µm BT differences in K, yellowish colours indicate the presence of ash.* ***Second line:*** *Figures on the left hand side show the ratio of radiances in channels 27 and 28, figures on the right hand side show TOMS SO_2 retrieval when available. For the Grimvston eruption, we show SCIAMACHY data instead. The location of the volcanoes is indicated by purple squares in the Terra/Aqua plots and a black triangle in the TOMS plots.*

Appendix 2: SO_2 quantity units.

A.1 Definition

A dobson unit is the most usual measure used in ozone research. The unit is named after G.M.B. Dobson, one of the first scientists to investigate atmospheric ozone (~1920 - 1960). He designed the 'Dobson Spectrometer' - the standard instrument used to measure ozone from the ground. The Dobson spectrometer measures the intensity of solar UV radiation at four wavelengths, two of which are absorbed by ozone and two of which are not.

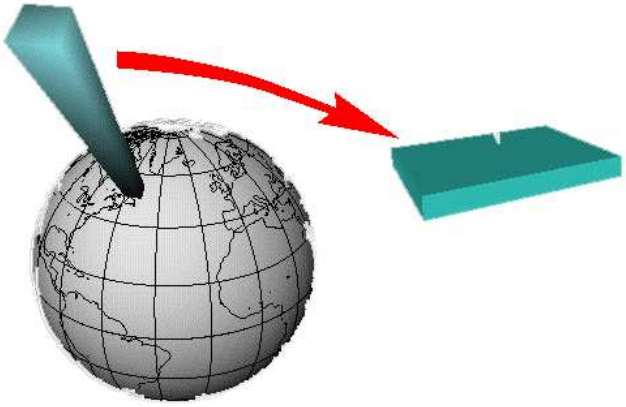

Figure 23: *a column of SO_2 containing 1 Dobson Unit (DU) would, at standard temperature and pressure, have a depth of 10^{-3} cm.*

One Dobson Unit (DU) is defined to be 0.01 mm thick at standard temperature and pressure. This unit can be used for any gas in the atmosphere. In the literature the SO_2 column is often given in DU. Note that *milli atm cm* (milli atmosphere per centimetre) is the same as the DU. This unit is also used in TOMS SO_2 retrievals.

Another unit for SO_2 measurement found in the literature is *ppmv* (part mixing ratio per million in volume). The definition here is that 1 *ppmv* of a gas corresponds to one part of gas per 1 million parts of air. The "v" denotes parts by volume (or equivalently by molecule or mol) in contrast to parts by mass.

A.2 Conversion from ppmv to DU

Let us define x as the mean mixing ratio of SO_2 (in ppmv) in a layer of depth Δz (in meters). P and T are the pressure and temperature of this layer, and P_0 and T_0 are the standard pressure and temperature (1013 hPa and 273.15 K, respectively). Knowing from the literature the SO_2 column in DU in case of a volcanic eruption, we can construct a SO_2 profile. The amount of SO_2 at each layer is expressed in ppmv. The column SO_2 DU being the sum of the DU present at each layer. The SO_2 thickness is therefore $\frac{x}{10^6}\Delta z$ at the ambient conditions, and $\left[\frac{x}{10^6}\frac{P}{P_0}\frac{T_0}{T}\right]\Delta z$ at standard conditions. x ppmv over a depth of Δz therefore corresponds to a column of $\left[\frac{x}{10^6}\frac{P}{P_0}\frac{T_0}{T}\right]\frac{\Delta z}{10^{-5}}DU$.

Appendix 3: Interesting websites

- http://www.temis.nl/aviation/so2.php
  http://www.oma.be/BIRA-IASB/Molecules/SO2archive/vs/

  TEMIS (Tropospheric Emission Monitoring Internet Service) aims to compute and deliver global concentrations of tropospheric trace gases and aerosol and UV products derived from observations of nadir-viewing satellite instruments such as GOME, SCIAMACHY and (A)ATSR. There is a part of the website containing a set of geographic regions covering known volcanoes and each of these regions is monitored. Concentrations of SO_2 are derived from UV measurements by satellite based instrument (SCanning Imaging Absorption SpectroMeter for Atmospheric CHartographY, SCHIAMACHY). If the concentrations in a given region exceed a limit, a warning is issued of a possible volcano eruption.

- http://toms.umbc.edu/
  SO_2 retrieved by TOMS/OMI instruments are stored in this website.

- http://modis.higp.hawaii.edu/
  Using infrared satellite data provided by the Moderate Resolution Imaging Spectroradiometer (MODIS), scientists at the Hawai'i Institute of Geophysics and Planetology, University of Hawai'i, have developed an automated system which maps the global distribution of thermal hot-spots in near-real-time, and displays the results on this website.

- http://www.volcano.si.edu/
  This is a general website on volcanoes. It is very useful to find volcanic locations, past eruptions, etc.

- http://volcanoes.usgs.gov/About/What/Monitor/Gas/CospecTraverse.html
  This website gives useful information on measuring volcanic SO_2 gas from the air with a Correlation Spectrometer.